Syst. Biol. 63(4):582–600, 2014
© The Author(s) 2014. Published by Oxford University Press, on behalf of the Society of Systematic Biologists. All rights reserved.
For Permissions, please email: journals.permissions@oup.com
DOI:10.1093/sysbio/syu022
Advance Access publication May 9, 2014

Integrating Incomplete Fossils by Isolating Conflicting Signal in Saturated and Non-Independent Morphological Characters

LILIANA M. DÁVALOS[1,2,*], PAÚL M. VELAZCO[3], OMAR M. WARSI[1], PETER D. SMITS[4], AND NANCY B. SIMMONS[3]

[1]*Department of Ecology and Evolution, Stony Brook University, 650 Life Sciences Building Stony Brook, NY 11794, USA,* [2]*Consortium for Inter-Disciplinary Environmental Research, School of Marine and Atmospheric Sciences, Stony Brook University, 129 Dana Hall, Stony Brook, NY 11794, USA,* [3]*Division of Vertebrate Zoology (Mammalogy), American Museum of Natural History, NY 10024, USA, and* [4]*Committee on Evolutionary Biology, University of Chicago, 1025 E. 57th Street, Culver Hall 402, Chicago, IL 60637, USA*

[*]*Correspondence to be sent to: Department of Ecology and Evolution, Stony Brook University, 650 Life Sciences Building, Stony Brook, NY 11794, USA; E-mail: liliana.davalos-alvarez@stonybrook.edu.*

Received 20 March 2013; reviews returned 28 May 2013; accepted 18 March 2014
Associate Editor: Mark Fishbein

Abstract.—Morphological characters are indispensable in phylogenetic analyses for understanding the pattern, process, and tempo of evolution. If characters are independent and free of systematic errors, then combining as many different kinds of characters as are available will result in the best-supported phylogenetic hypotheses. But since morphological characters are subject to natural selection for function and arise from the expression of developmental pathways, they may not be independent, a situation that may amplify any underlying homoplasy. Here, we use new dental and multi-locus genetic data from bats (Mammalia: Chiroptera) to quantify saturation and similarity in morphological characters and introduce two likelihood-based approaches to identify strongly conflicting characters and integrate morphological and molecular data. We implement these methods to analyze the phylogeny of incomplete Miocene fossils in the radiation of Phyllostomidae (New World Leaf-nosed Bats), perhaps the most ecologically diverse family of living mammals. Morphological characters produced trees incongruent with molecular phylogenies, were saturated, and showed rates of change higher than most molecular substitution rates. Dental characters encoded variation similar to that in other morphological characters, while molecular characters encoded highly dissimilar variation in comparison. Saturation and high rates of change indicate randomization of phylogenetic signal in the morphological data, and extensive similarity suggests characters are non-independent and errors are amplified. To integrate the morphological data into tree building while accounting for homoplasy, we used statistical molecular scaffolds and combined phylogenetic analyses excluding a small subset of strongly conflicting dental characters. The phylogenies revealed the Miocene nectar-feeding †*Palynephyllum* nests within the crown nectar-feeding South American subfamily Lonchophyllinae, while the Miocene genus †*Notonycteris* is sister to the extant carnivorous *Vampyrum*. These relationships imply new calibration points for timing of radiation of the ecologically diverse Phyllostomidae. [Chiroptera; conflict; dentition; morphology; Phyllostomidae; saturation; scaffold; systematic error.]

Fossil remains provide crucial data for understanding the pattern, process, and tempo of evolution (Wiens et al. 2010; Ronquist et al. 2012a), and for this reason phylogenetic analyses of morphological characters are indispensable. Combining data from as many character systems as are available can also provide the most powerful inference of phylogeny, and the strongest test of evolutionary hypotheses (de Queiroz and Gatesy 2007; Hermsen and Hendricks 2008). This rationale for integrating morphological data through combination crucially depends on both the absence of systematic error and independence among characters (de Queiroz and Gatesy 2007; Springer et al. 2007). However, different character systems may have different properties of phylogenetic signal (e.g., arising from very different rates of evolution or the influence of natural selection). Integrating these systems in phylogenetic analyses then requires accounting for these differences (Wake 1991; Kangas et al. 2004; Eick et al. 2005; Springer et al. 2007).

When analyses fail to accurately model evolutionary processes (e.g., by assuming neutral evolution when a character is under selection), additional data may mislead through bias. This is called systematic error (Phillips et al. 2004). Systematic errors have been found when constraints on character states in nucleotides and multiple substitutions at the same site produce end states that are random with respect to shared history (Simmons and Freudenstein 2003), when mutational biases are incorrectly modeled (Gruber et al. 2007), if natural selection for a specific function has resulted in adaptive convergence (Li et al. 2008; Liu et al. 2010), and when correlated evolution at nearby sites violates the assumption of independence implicit in most phylogenetic analyses (Davis et al. 2009). Ceilings on the number of character states, misleading adaptive convergence, and character dependency have all been observed in morphological characters (Wagner 2000; Wiens et al. 2003; Kangas et al. 2004; Dávalos et al. 2012). Further, evolutionary adaptation is expected to shape morphological characters to a greater extent than many nucleotide substitutions because all morphological characters are phenotypic (Wake 1991; Springer et al. 2007; 2008). Nonetheless, the potential for systematic error to mislead morphological phylogenies and undermine data combination has not been as thoroughly explored as it has with molecular data. Crucially, comparisons among loci and models that account for biased data make systematic error more tractable with molecular data (Muse and Gaut 1994; Gruber et al. 2007; Blanquart and Lartillot 2008; Davies et al. 2012).

Molecular scaffolds in which trees derived from molecular sequence analyses are used to constrain searches for optimal morphological trees were developed as a way to integrate data under the

Downloaded from https://academic.oup.com/sysbio/article/63/4/582/1623176 by guest on 20 August 2022

assumption that morphological characters may be too homoplasious to be directly analyzed (Springer et al. 2001; 2007). Morphologists and paleontologists have criticized scaffolds because they fail to convey phylogenetic uncertainty arising from both the molecular and morphological data, and assign much greater weight to molecular sequences *a priori* (Manos et al. 2007; Hermsen and Hendricks 2008). By not analyzing all characters on equal footing, scaffolds overlook potential support in molecular data sets for clades strongly supported by morphology (de Queiroz and Gatesy 2007).

As models to analyze morphological characters have been proposed, developed, and extended to include relaxed-clock analyses (Lewis 2001; Pyron 2011; Ronquist et al. 2012a), the question of how to integrate morphological characters in phylogenetic analyses has become more pressing. Beyond providing constraints for dating divergence and understanding the tempo and mode of trait evolution, morphological characters can also contribute to understanding the evolution of extant taxa (Wiens 2004). In some cases, including fossil taxa in combined analyses may actually change perceived relationships among extant lineages (Manos et al. 2007; Hermsen and Hendricks 2008). Uncovering errors in morphological data and improving methods to integrate and analyze morphological characters are therefore of great importance to fully inferring and analyzing the Tree of Life (Wiens 2009).

In this study, we introduce and analyze multi-locus DNA sequences and a set of >270 dental characters for the mammalian family Phyllostomidae with the goal of investigating the phylogenetic signal and features of morphological data. Phyllostomid bats are perhaps the single most ecologically diverse mammalian family, including specialized lineages that feed exclusively on nectar, blood, hard or soft fruits, in addition to taxa that are carnivores and/or gleaning insectivores (Rojas et al. 2011; Santana et al. 2011; Dumont et al. 2012). Fossil phyllostomids are known from the middle Miocene of northern South America (Czaplewski et al. 2003b) and extensive Pleistocene deposits in Central and South America, and the Caribbean (Czaplewski et al. 2003a; Fracasso and Salles 2005; Dávalos and Russell 2012; Dávalos and Turvey 2012). The outstanding diversity of phyllostomids makes the evolution of their taxonomic diversity, feeding specializations, and biogeography of interest to systematists, evolutionary ecologists, and functional morphologists (Rojas et al. 2011, 2012; Dumont et al. 2012; Santana et al. 2012). The phylogenetic placement of Miocene fossils, in particular, is critical to understanding the tempo of phyllostomid diversification. To date, only one analysis including one (of three) Miocene fossil lineages has ever been conducted, and it encompassed only 7 of 58 extant genera (Czaplewski et al. 2003b). Successfully integrating morphological characters into our analyses is therefore crucial to understanding the evolution of phyllostomids.

Given their outstanding ecological diversity in a single unarguably monophyletic group, phyllostomids are uniquely suited for testing for signals of systematic error in morphological characters driven by functional and developmental constraints (Springer et al. 2007). Since these constraints affect multiple traits simultaneously (Wiens et al. 2003; Kangas et al. 2004; Carrier et al. 2005), combinations of character states will end up being similar to one another and the observed signal will amplify any underlying errors. The occurrence of identical character states that do not arise by common descent but by other processes is homoplasy. One form of homoplasy involves rates of change so high that the observed distribution of states cannot be distinguished from a random assignment, and this can be diagnosed by examining saturation in character state changes. Specifically, in this study we aimed to: (1) measure saturation and similarity in morphological characters, as well as phylogenetic conflict with molecular trees; (2) find ways to locate phylogenetic conflicts among morphological characters (if substantial homoplasy is detected); and (3) extend methods to integrate morphological data with molecular sequence data to account for systematic errors uncovered.

Materials and Methods

Taxonomic Sampling

Phyllostomidae (Mammalia: Chiroptera: Noctilionoidea) is a group of Neotropical bats whose monophyly is strongly supported by both morphological and molecular synapomorphies (Simmons 1998; Baker et al. 2000, 2003; Wetterer et al. 2000). Phyllostomid bat species were traditionally classified into subfamilies based on dietary habits and associated morphologies (Wetterer et al. 2000). We sampled densely among lineages characterized by insectivory and nectarivory because Miocene fossils (†*Palynephyllum*, †*Notonycteris*) have been assigned to groups sharing these dietary specializations based on similarity to extant taxa and, for †*Notonycteris*, analyses of 48 dental characters in seven genera (Czaplewski et al. 2003b). Two subfamilies formerly recognized based on morphological characters and later shown by molecular data to be paraphyletic were sampled. The subfamily Glossophaginae *sensu* Wetterer et al. (2000) comprised primarily nectarivorous lineages whose morphological synapomorphies are associated with feeding ecology, implying ecological convergence (Dávalos et al. 2012). This group has subsequently been divided into two monophyletic groups, Glossophaginae *sensu stricto* and Lonchophyllinae (Baker et al. 2003). No similar patterns of support from ecologically driven character changes have been found for the subfamily Phyllostominae *sensu* Wetterer et al. (2000), another group shown to be paraphyletic with molecular data (Baker et al. 2003; Datzmann et al. 2010). Lineages of phyllostomines *sensu* Wetterer et al. (2000) retain the primitive feeding ecology of insectivory (Rojas et al. 2011).

Downloaded from https://academic.oup.com/sysbio/article/63/4/582/1623176 by guest on 20 August 2022

Sampling densely among primarily nectarivorous and insectivorous lineages enabled inclusion of all the potential relatives of four fossil species. Three of these taxa are extremely incomplete Miocene fossil taxa—†*Notonycteris magdalenensis*, †*N. sucharadeus*, and †*Palynephyllum antimaster*—known only from isolated teeth, partial mandibles, and partial postcranial bones. We also included the better-preserved Quaternary †*Phyllonycteris major* (Choate and Birney 1968). Six additional noctilionoid species in the families Mormoopidae, Noctilionidae, and Thyropteridae were included as outgroups. *Thyroptera tricolor* (Chiroptera: Thyropteridae) was used to root trees. The total number of genera sampled was 50, with both morphological and molecular data for 85 extant species. An additional 28 species were represented only by morphological data including fossils and extant species and subspecies known only from the type of material and lacking tissue vouchers at this time.

Morphological Data

The new morphological data generated to place the fossils comprised representatives of all currently recognized phyllostomid subfamilies, including 107 species and subspecies in 46 phyllostomid genera. We identified 278 dental characters of potential phylogenetic significance based on comparisons among ingroup taxa. Characters were generated using reductive character coding *sensu* Wilkinson (1995). We used combinations of two character states to indicate taxonomic polymorphism in composite terminal taxa (species or subspecies). Of the 278 characters scored, 112 were treated as ordered in phylogenetic analyses. These multistate characters describe apparently progressive gradations in size, shape, or relative position, and were coded as ordered to preserve hypotheses of homology of states and transformations. We assembled the morphological matrix using MorphoBank (www.morphobank.org), a public online database for assembling and managing morphological matrices (O'Leary and Kaufman 2012). Each cell in the matrix is documented with a labeled image that can be zoomed into or downloaded to better observe the structure in question. The morphological matrix is available at MorphoBank as project P891.

Overview

Our analyses aimed to find the best way to investigate the data structure of morphological data and integrate morphological characters with DNA sequences. Figure 1 summarizes these analyses of morphological character structure and data integration and serves as a general guide to the methods implemented here.

Measuring saturation in morphological character state changes.—A maximum parsimony (MP) phylogenetic approach and curve fitting were used to assess the extent of saturation in changes in morphological character states using the state: step relationship (Fig. 1, upper right; Wagner 2000). Saturation indicates one kind of homoplasy, as character states end up being identical without common descent (Dávalos et al. 2012). To quantify saturation, we first inferred a morphological phylogeny using the Unix version of PAUP* v. 4b10 (Swofford 2002) in MP heuristic searches including ordered characters and 1000 replicates of random sequence addition, followed by tree–bisection–reconnection (TBR). All maximally parsimonious trees were retained.

The goal of the state: step plot is to test the hypothesis that new character states accumulate continuously throughout evolutionary history. Character optimization and ordering could affect this relationship: accelerated transformation (acctran) would place changes earlier in the evolutionary history of the clade, and ordered steps would lengthen the tree compared with unordered steps. These choices would skew results in the direction of rejecting the null hypothesis of continuous accumulation of character states. For this reason, the resulting trees were used to optimize morphological character state changes using the delayed transformation option (deltran) and all unordered characters. Each step of the MP phylogenies beginning with the first transformation starting from the root was then matched to its beginning and end character state. We could then determine whether the end character state had been previously observed or not. The age of each node was determined by the relative branching of the MP morphological phylogenies, and when identical relative ages were found, using the dates of divergence estimated by Dumont et al. (2012).

The resulting table includes the step in the phylogeny, the cumulative number of character states observed, and whether or not that particular step resulted in a new state or not (Supplementary Table S1, http://dx.doi.org/10.5061/dryad.pg4c0). The steps of the phylogeny were divided into two sets: those that result in new states and those that do not. If new character states were distributed throughout the sequence of steps in the MP tree, then there should be no significant difference in the distributions of step numbers from both groups. That is, if new character states are equally probable throughout evolutionary history, then steps that result in new states should not be concentrated at low or high step numbers, and both kinds of steps would have similar step ranks. We tested this null hypothesis using a Wilcoxon signed-rank test (Wilcoxon 1945) as implemented in R v.2.15.1 (R Development Core Team 2012). The inflection point beyond which the accumulation of new character states slows down relative to the steps of the phylogeny was identified by fitting a segmented linear model using the *segmented* R package v.0.2-9.4 (Muggeo 2008). We compared predictions from two hypotheses of non-linear accumulation of character states: a finite-state models in which there is an upper boundary

Downloaded from https://academic.oup.com/sysbio/article/63/4/582/1623176 by guest on 20 August 2022

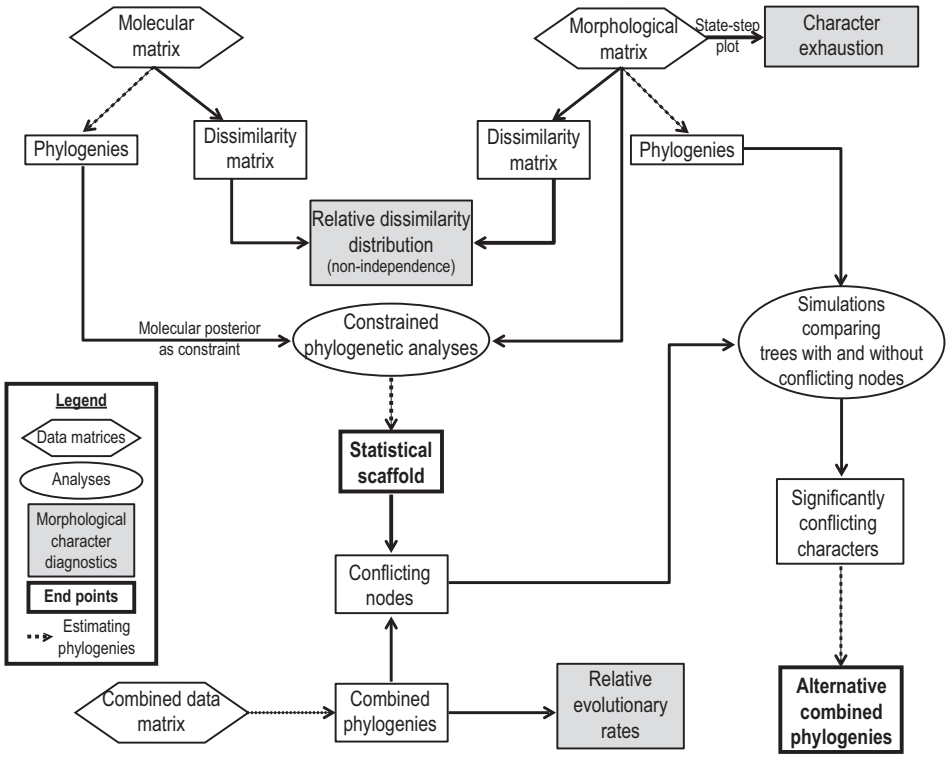

FIGURE 1. Graphic summary of analyses performed to estimate character state exhaustion in morphological characters, quantify rates of evolution in molecular and morphological partitions, and integrate molecular and morphological data. The workflow begins with molecular and morphological data matrices, and subsequent analyses: (1) examine saturation and independence in the morphological data (upper right), (2) examine character independence (upper center), (3) build a phylogenetic constraint from molecular sequences and produce a constrained integrated phylogeny or statistical scaffold (left half), (4) generate unconstrained combined phylogenies (lower left), (5) identify nodes that conflict between constrained and unconstrained phylogenies (middle center), and (6) use conflicting nodes and simulations to identify outlier morphological characters supporting conflicting nodes and exclude these from an alternative set of combined phylogenies (middle and lower right).

on the total number of character states, and the ordered-state model in which each state has a finite number of descendent states (Wagner 2000). Non-linear relationships describing the finite-state and ordered-state hypotheses were fitted to the data using the equations of Dávalos et al. (2012) and the *nls* command in R (Fig. 1, upper right). The fit of the non-linear models to the data was compared using the Akaike Information Criterion (AIC), with a lower AIC indicating better fit of the curve to the data (Burnham and Anderson 2002).

Quantifying similarity between characters.—Selection for function under similar ecological pressures has been proposed as the mechanism producing adaptive convergence in character states (Wiens et al. 2003; Springer et al. 2007). Correlations between morphological character states resulting from development are also expected to generate homoplasy by limiting both character states and combinations of character states (Wake 1991). Both of these mechanisms are known to operate on mammalian dentition (Kangas et al. 2004; Evans et al. 2007) and will result in non-independence of character states. To explore the independence of character states, we calculated the Gower pairwise dissimilarity among all morphological and molecular characters (Gower 1966). The Gower dissimilarity has been adopted in community ecology and genomics, transcriptomics, and proteomics to explore correlations in variables comprising continuous measures, categories (e.g., different base pairs), binaries, and ordinals (Legendre and Gallagher 2001; Marengo et al. 2003; Peterson 2003; Alheit et al. 2011). It ranges from 0 to 1, with 0 indicating complete identity and 1 complete dissimilarity in patterns found in pairs of variables.

The coding of states using similar symbols from one morphological character to the next does not imply an equivalence of states between characters. To overcome this challenge posed by morphological data, we recoded each character as a binary matrix of similarity and difference between species. For example, if a morphological character had states 0012 for the first four species, the comparison between the first two species would yield a 0; between species 2 and 3, a 1; and between species 3 and 4, a 1. This transformation made all recoded characters directly comparable to one another, and Gower dissimilarities were calculated from these recoded characters.

To generate dissimilarity distributions comparable between morphological and molecular data, invariable

Downloaded from https://academic.oup.com/sysbio/article/63/4/582/1623176 by guest on 20 August 2022

base pairs were excluded from calculations. All ambiguous characters of both kinds of data were converted to empty cells, and nucleotides were coded as categorical variables. The *daisy* command in the *cluster* R package v.1.14.3 (Maechler et al. 2012) was then used to calculate the Gower dissimilarities (Fig. 1, upper center). This implementation ignored missing values in calculating the dissimilarities for a given row of characters. The frequency distributions of dissimilarities were then compared by plotting histograms and by estimating and visualizing the relative frequency distribution using the R package *reldist* v.1.6-1 (Handcock and Morris 1999; Handcock 2013).

Molecular Data

Small pieces of tissue (~2–10 mg) were used for DNA extraction using the QIAmp DNA Micro Kit (Qiagen N.V. Catalogue no. 56304). To maximize DNA recovery, we followed the manufacturer's tissue protocol with an extra step of using carrier RNA after lysis. All DNA was eluted in molecular-grade water. DNA yields from tissue extractions ranged from 20–100 ng/μl.

We collected new partial sequences from seven nuclear loci: two introns, *thy* or thyrotropin beta chain, *stat5a* or signal transducer and activator of 5A; one 3′-untranslated region (UTR), *plcb4* or phospholipase C beta 4; three autosomal exons, *bdnf* or brain-derived neurotrophic factor, *ttn6* or titin 6, *rag2* or recombination-activating protein 2; and the X-chromosome exon *atp7a* or ATPase-7A. New complete sequences were generated for the mitochondrial locus *cytb* or cytochrome b. To maximize sampling of nectarivorous lineages, published sequences from the mitochondrial genes *cox1* or cytochrome oxidase I, *cytb*, and the ribosomal RNAs 12S, $tRNA^{val}$ and 16S were also included (Baker et al. 2003; Clare et al. 2007; 2011). All sequences analyzed in this study are shown in Table 1.

We used primers designed by Eick et al. (2005) to amplify and sequence introns, those by Teeling et al. (2005) for the 3′-UTR, those by Murphy and O'Brien (2007) for the nuclear exons; and the combination of primers by Jansa et al. (1999) to amplify the *cytb* gene. To increase efficiency in amplification with noctilionoid taxa, we redesigned the *bdnf* and *ttn6* primers, and used newly designed internal primers for sequencing the *ttn6* locus. All primers used in this study are shown in Supplementary Table S2. Touchdown PCR amplifications were used for all genes, except *thy*, for which a single annealing temperature was used (Supplementary Tables S3 and S4). All amplifications were carried out using the *Taq* PCR Core Kit (Qiagen N.V. Catalogue no. 201223) with the reagent mix shown in Supplementary Table S5. Fragments were cycle- sequenced in both directions using external and sometimes internal primers (Supplementary Table S2). Automated Applied Biosystems 3730 sequencers were used to analyze the sequenced fragments. Contigs were aligned using the assembly tool in Geneious v.5.3.6 (Drummond et al. 2011). Quality scores and visual inspection of chromatograms were used to identify heterozygous positions.

Alignment.—We used the Perl script transAlign v1.2 (Bininda-Emonds 2005) to align all nuclear exons and protein-coding mitochondrial genes. The multiple sequence alignment method multiple alignment through fast Fourier transform (MAFFT) v6.710b applying the *einsi* protocol was used to align non-coding nuclear sequences (Katoh et al. 2005; Katoh and Toh 2008). An alignment of mitochondrial ribosomal RNA (mtrDNA) sequences based on the secondary structure of the genes was obtained directly from Dávalos et al. (2012). After trimming ends to reduce missing data, the concatenated alignment comprised 9584 base pairs.

Selection of partition scheme and optimal models of DNA evolution.—The molecular data were divided into genomic and functional partitions. The maximum number of partitions (nine data blocks) comprised three codon positions each for mitochondrial and nuclear protein-coding genes, mtrDNA loops and stems, and introns together with one 3′ UTR. The optimal partitioning scheme and model of DNA evolution for individual partitions were selected using the Bayesian Information Criterion (BIC) in the PartitionFinder python script v.1.0.0 (Lanfear et al. 2012). Briefly, PartitionFinder takes the predefined partitions in the alignment and compares combinations of data blocks and models of evolution for those data blocks using ML phylogenies as implemented in PhyML (Guindon et al. 2010). The approximate gamma distribution accommodates sites with very low rates of change (Yang 1994). To avoid possible dependencies between gamma and the proportion of invariable sites (Gu et al. 1995), the range of models of sequence evolution was restricted to either parameter, but not both. The greedy algorithm, which uses the BIC to guide the search for optimal partitioning schemes, was used to reduce computational time. Results from PartitionFinder comprised both the optimal partitioning scheme and the best-fit models of evolution for its individual partitions, and these were applied in subsequent ML and Bayesian phylogenetic analyses. Downstream analyses included tree topology and branch length searches. Partitioned alignments and resulting trees were deposited in TreeBASE under ID 13970.

Phylogenetic Analyses

The central goal of our phylogenetic analyses was to integrate morphological and molecular data (Fig. 1). Two approaches were used: (1) statistical molecular scaffolds and (2) combined analyses. Previous analyses have used a phylogeny derived from molecular data as a backbone constraint in MP searches using morphological data—a molecular scaffold (Springer et al. 2001; Manos et al. 2007). Besides *a priori* assigning greater weight

Downloaded from https://academic.oup.com/sysbio/article/63/4/582/1623176 by guest on 20 August 2022

to molecular sequences (Hermsen and Hendricks 2008), this approach has two disadvantages. First, it does not account for the phylogenetic uncertainty associated with the summary molecular phylogeny, as a single majority-rule consensus tree resulting from MP bootstrap analyses is generally used (Springer et al. 2001; Manos et al. 2007). Second, measures of branch support for the morphological data are superimposed on the molecular scaffold phylogeny through bootstraps or matrix representation parsimony, again losing the phylogenetic uncertainty associated with both types of data. We extended the scaffolding approach to overcome both of these issues by generating statistical scaffolds. With our approach morphological characters may influence the phylogeny of taxa represented in molecular posterior phylogenies if these are in poorly supported nodes, but not if nodes are strongly supported.

Statistical molecular scaffolds.—A combination of Bayesian and ML approaches were used to obtain statistical molecular scaffolds (Fig. 1, left half). First, a posterior distribution of molecular phylogenies was obtained through Metropolis-coupled Markov chain Monte Carlo Bayesian analyses applying the best partitioning scheme and optimal models of sequence evolution for each partition using MrBayes v.3.2.0 (Ronquist et al. 2012b). Most MrBayes runs were completed in the CIPRES Science Gateway (Miller et al. 2010). Nucleotide frequencies, shape of the discrete approximation of the gamma distribution of rates across the alignment, transition/transversion rate ratios, and rate matrix parameters were all unlinked between partitions; and the rate of evolution was allowed to vary between partitions (*prset ratepr = variable*). Four independent searches ran for 10 million generations with a starting tree derived from maximum likelihood (ML) analyses. This starting tree was obtained through a ML search using the Randomized Axelerated ML (RAxML) algorithm v.7.2.7 (Stamatakis 2006). The preliminary analysis was conducted on a maximally partitioned alignment (nine data blocks) and implemented the general time reversible (GTR) model of nucleotide evolution with a discrete approximation of a gamma distribution to account for variation in rates between sites for all data blocks (Tavaré 1986; Yang 1994).

To improve chain mixing, the temperature of the heated chains was lowered from the MrBayes default of 0.02 to 0.01. Burn-in of Bayesian searches was assessed by examining log-likelihood and tree length estimates using Tracer v.1.5 (Rambaut and Drummond 2007). Convergence within searches was assessed through the standard deviations of split frequencies, and between searches by comparing posterior estimates of log-likelihood, tree lengths, and relative rate parameters. Standard deviations of split frequencies <0.01 were interpreted as indicative of within-search convergence. Parameters were assessed to have converged between runs if their median posterior distributions differed by no more than 1 standard deviation from one another. Estimates of autocorrelation time between posterior samples were used to subsample posterior phylogenies to obtain an uncorrelated posterior sample of 1000 phylogenies.

Second, each phylogeny in the uncorrelated posterior sample of Bayesian molecular phylogenies was used as a backbone constraint in ML searches in RAxML using the Markov k-state variable model with a gamma distribution of rate variation among characters to analyze the morphological data (Mkv + gamma) (Fig. 1; Lewis 2001). Branch lengths and model parameters for the combined data were optimized on each resulting tree using a partition file specifying different rate matrices and approximate gamma distribution for each molecular partition, and the Mkv+gamma model for the morphological model (i.e., f *e*, -t *each_tree*, -q *file_with_partitions*, -s *combined_data*, and -K *MK* commands). The resulting trees were then summarized into a maximum clade credibility tree with median branch lengths using TreeAnnotator v.1.6.1 (Rambaut and Drummond 2010).

Unconstrained combined data analyses.—The unconstrained combined morphological and molecular data set were analyzed using ML and Bayesian approaches. To obtain a ML estimate of the combined phylogeny, we used RAxML with a partition file, and the Mkv+gamma model to analyze the morphological data. The rapid bootstrap algorithm of RAxML was followed by thorough ML searches (i.e., f *a*, -q *file_with_partitions*, -s *combined_data*, and -K *MK* commands) (Stamatakis et al. 2008). One hundred bootstrap pseudoreplicates were used to estimate branch support.

Bayesian estimates of phylogeny were obtained by running four independent analyses for 10 million generations with the optimal molecular partition scheme, the best-fit models of sequence evolution, and unlinked parameters for partitions (Fig. 1, lower left and center). The Mkv+gamma model of evolution with symmetric rates of change between character states (default, or *Prset symdirihyperpr = fixed(infinity)*) was used to analyze the morphological partition. Burn-in and convergence were assessed as with the molecular data set (see the "Statistical molecular scaffolds" section). The temperature of the heated chains was lowered to 0.001 to improve chain mixing.

Analyses of morphological data.—To make our analyses comparable to the majority of published morphological phylogenies (e.g., Wetterer et al. 2000; Dávalos et al. 2012), we analyzed the morphological data using MP, ML, and Bayesian methods. MP heuristic searches used 20 replicates of random sequence addition followed by TBR in PAUP*. ML optimizations applied the Mkv+gamma model in 100 searches using the rapid bootstrap algorithm followed by a thorough search for the optimal tree. Three independent Bayesian analyses ran for 40 million generations with the Mkv+gamma model of character evolution and a prior on the distribution of

Downloaded from https://academic.oup.com/sysbio/article/63/4/582/1623176 by guest on 20 August 2022

TABLE 1. Species and GenBank accession numbers for each locus analyzed

Species	*atp7a*	*bdnf*	*plcb4*	*rag2*	*stat5a*	*thy*	*ttn6*	12S, tRNA^{val}, 16S	*cox1*	*cytb*
Anoura caudifer	KC783005	KC782952	KC783058	KC783112	—	KC783214	KC783123	AY395835	EF079981	L19506
Anoura geoffroyi	AY834495	AY834519	AY835951	AF316431	—	—	AY834718	—	EF079996	FJ155495
Anoura latidens	—	—	—	—	—	—	—	—	EF080020	—
Artibeus gnomus	KC783006	KC782953	KC783059	—	KC783173	—	KC783124	—	EF080067	EU160957
Artibeus jamaicensis	KC783007	KC782954	KC783060	FN641674	KC783174	KC783215	KC783125	AF061340	AF061340	GQ861667
Artibeus lituratus	KC783008	KC782955	KC783061	—	—	KC783216	KC783126	—	EF080083	AY684740
Artibeus obscures	—	KC782956	KC783062	—	—	KC783217	KC783127	—	EF080106	—
Brachyphylla cavernarum	KC783010	KC782957	KC783063	AF316436	KC783175	—	KC783128	AY395806	—	AY620467
Brachyphylla nana	—	—	FN643251	—	—	—	—	—	—	AY620444
Carollia brevicauda	KC783011	KC782958	KC783064	KC783113	KC783176	—	KC783129	—	JF453684	AF511951
Carollia perspicillata	KC783012	KC782959	KC783065	KC783114	KC783177	KC783218	KC783130	AY395836	EF080211	FJ589715
Choeroniscus godmani	—	—	—	AF316440	—	—	—	—	EU096698	—
Choeroniscus minor	KC783013	KC782960	KC783066	—	—	KC783219	KC783131	—	EF080294	KC783055
Choeronycteris Mexicana	—	—	—	—	—	—	—	AY395808	—	—
Chrotopterus auritus	KC783014	KC782961	KC783067	AF316442	KC783178	KC783220	KC783132	AF411538	EF080303	KC783057
Desmodus rotundus	KC783015	KC782962	KC783068	AF316444	KC783179	KC783221	KC783133	AF263228	JF435307	FJ847517
Diaemus youngi	—	—	—	AF316445	—	—	—	AF411534	EF080328	FJ155475
Diphylla ecaudata	—	KC782963	KC783069	KC783115	KC783180	—	KC783134	AF411533	—	DQ077399
Enchisthenes hartii	KC783016	KC782964	KC783070	AF316449	—	KC783222	—	AY395838	EU161064	U66517
Erophylla bombifrons	—	—	—	—	—	—	—	—	—	GU937269
Erophylla sezekorni	KC783017	KC782965	KC783071	AF316450	KC783181	KC783223	KC783135	AY395839	—	GU937254
Glossophaga commissarisi	—	—	—	—	—	—	—	—	—	AF382886
Glossophaga longirostris	—	—	—	—	—	—	—	—	JF459162	AF382875
Glossophaga morenoi	—	—	—	—	—	—	—	—	—	AF382882
Glossophaga soricina	KC783018	—	KC783072	AF316452	KC783182	AJ865666	KC783136	AY395840	EF080360	AF423081
Glyphonycteris daviesi	KC783019	KC782966	KC783073	AF316464	KC783183	KC783224	KC783137	AY395812	EF080364	AY380747
Glyphonycteris sylvestris	—	—	FN643258	AF316471	—	—	—	AY395841	EF080366	AY380746
Hylonycteris underwoodi	—	—	FN643259	AF316453	—	—	—	AY395813	—	—
Lampronycteris brachyotis	KC783020	KC782967	KC783074	AF316463	KC783184	KC783225	KC783138	AF411536	EF080370	AY380748
Leptonycteris curasoae	—	—	FN643260	—	—	—	—	—	—	AF382889
Lichonycteris obscura	—	—	—	—	—	—	—	—	JF448853	—
Lionycteris spurrelli	—	KC782968	KC783075	—	—	KC783226	—	AY395815	EF080374	AF423100
Lonchophylla handleyi	—	—	—	—	—	—	—	—	—	AF423094
Lonchophylla mordax	—	—	—	KC783116	KC783185	—	KC783139	—	—	AF423095
Lonchophylla robusta	—	—	FN643261	FN641677	—	—	—	—	—	AF423091
Lonchophylla thomasi	KC783021	KC782969	KC783076	AF316456	KC783186	KC783227	KC783140	AY395842	EF080377	AF423086
Lonchorhina aurita	KC783022	KC782970	KC783077	KC783117	—	KC783228	KC783141	AY395843	—	FJ155494
Lonchorhina orinocensis	—	KC782971	KC783078	—	—	—	KC783142	—	—	—
Lophostoma brasiliense	KC783023	KC782972	KC783079	AF316489	KC783187	KC783229	KC783143	AF411544	HQ545592	FJ155486
Lophostoma carrikeri	KC783024	KC782973	KC783080	KC783118	KC783188	KC783230	KC783144	—	EF080429	—
Lophostoma evotis	—	—	—	AF442080	—	—	—	—	—	FJ155491
Lophostoma schulzi	KC783025	KC782974	KC783081	AF442079	KC783189	KC783231	KC783145	—	EF080432	FJ155485
Lophostoma silvicolum	KC783026	KC782975	AY835949	—	—	KC783232	KC783146	AF263230	—	—

(*Continued*)

Downloaded from https://academic.oup.com/sysbio/article/63/4/582/1623176 by guest on 20 August 2022

TABLE 1. Continued.

Species	*atp7a*	*bdnf*	*plcb4*	*rag2*	*stat5a*	*thy*	*ttn6*	12S, tRNA^{val}, 16S	*cox1*	*cytb*
Macrophyllum macrophyllum	KC783027	KC782976	KC783082	—	KC783190	KC783233	KC783147	AF411540	EU096773	FJ155484
Macrotus californicus	—	—	KF471662	AF316459	KF471663	—	—	—	—	AY380744
Macrotus waterhousii	KC783028	KC782977	KC783083	KC783119	KC783191	KC783234	KC783148	AF263229	—	—
Micronycteris brosseti	—	—	—	—	—	—	—	—	—	AY380771
Micronycteris hirsuta	KC783029	KC782978	KC783084	AF316465	KC783192	KC783235	KC783149	AY395819	EF080447	AY380769
Micronycteris homezi	—	—	—	—	—	—	—	—	—	AY380754
Micronycteris matses	KC783030	KC782979	KC783085	KC783120	—	KC783236	KC783150	—	—	DQ077419
Micronycteris megalotis	KC783031	KC782980	KC783086	AF316467	KC783193	—	KC783151	AY395821	EU096780	DQ077426
Micronycteris microtis	KC783032	KC782981	KC783087	—	KC783194	KC783237	KC783152	—	—	AY380756
Micronycteris minuta	KC783033	KC782982	KC783088	—	KC783195	—	—	AY395823	—	AY380752
Micronycteris schmidtorum	KC783034	KC782983	KC783089	AF316470	KC783196	KC783238	KC783153	—	—	DQ077406
Mimon cozumelae	—	KC782984	KC783090	—	KC783197	—	KC783154	—	—	—
Mimon crenulatum	KC783035	—	KC783091	—	EU652033	—	KC783155	AF411543	EU096781	FJ155478
Monophyllus plethodon	—	—	—	—	—	—	—	—	—	AF382887
Monophyllus redmani	KC783036	KC782985	KC783092	—	KC783198	—	KC783156	—	—	AF382888
Mormoops blainvillei	KC783037	KC782986	KC783093	AY028169	KC783199	KC783239	KC783157	—	—	AF338686
Musonycteris harrisoni	—	—	—	AF316475	—	—	—	AY395844	—	—
Noctilio albiventris	KC783038	AY834520	KC783094	AF330811	KC783200	gAJ865658	KC783158	—	EF080524	AF330806
Noctilio leporinus	KC783039	KC783004	KC783095	AF330816	KC783201	KC783240	KC783159	AF263224	EF080534	AF330796
Phylloderma stenops	—	KC782987	KC783096	AF316480	—	KC783241	—	AF411542	EU096830	FJ155480
Phyllonycteris aphylla	—	—	—	AF316478	—	—	—	—	—	AF187033
Phyllonycteris poeyi	KC783040	KC782988	KC783097	KC783121	KC783202	KC783242	KC783160	—	—	GU937240
Phyllostomus discolor	—	—	—	—	—	—	—	—	EF080546	—
Phyllostomus elongatus	KC783041	—	KC783098	—	KC783203	—	KC783161	—	EF080551	KC783056
Phyllostomus hastatus	KC783042	—	KC783099	—	EU652033	KC783243	KC783162	AF411541	EF080556	FJ155479
Platalina genovensium	—	—	—	—	—	—	—	—	—	AF423101
Platyrrhinus helleri	KC783043	KC782991	KC783100	AF316481	KC783204	KC783244	KC783163	—	EF080579	FJ154140
Pteronotus davyi	KC783044	KC782992	KC783101	AF338692	KC783205	KC783245	KC783164	AF407176	—	AF338671
Pteronotus parnellii	KC783045	—	KC783102	KC783122	KC783206	KC783246	—	—	—	AF338661
Pygoderma bilabiatum	KC783046	KC782994	KC783103	AF316483	—	KC783247	KC783166	AY395826	—	AY604438
Rhinophylla alethina	—	—	—	—	—	—	—	—	—	AF187028
Rhinophylla fischerae	—	—	—	—	—	—	—	—	—	AF187032
Rhinophylla pumilio	KC783047	KC782995	KC783104	AF316484	KC783207	EU371960	KC783167	AY395827	EF080598	AF187031
Sturnira lilium	KC783048	KC782996	KC783105	—	KC783208	KC783248	—	—	EF080684	DQ312398
Thyroptera tricolor	AY834502	KC782997	KC783106	—	KC783209	KC783249	AY834725	AF263233	—	—
Tonatia saurophila	KC783049	KC782998	KC783107	AF442086	KC783210	KC783250	KC783169	AF411530	EF080734	—
Trachops cirrhosus	KC783050	KC782999	FN643273	—	AJ865422	KC783251	—	AF411539	EF080747	FJ155483
Trinycteris nicefori	KC783051	KC783000	KC783108	—	KC783211	KC783252	KC783170	AY395830	—	—
Uroderma bilobatum	KC783052	KC783001	KC783109	AF316491	—	EU371973	KC783171	AY395831	EF080788	AY169955
Vampyrodes caraccioli	KC783053	KC783002	KC783110	AF316494	KC783212	EU371991	—	AY395846	EF080804	AY157034
Vampyrodes major	—	—	—	—	—	—	—	—	—	HQ637422
Vampyrum spectrum	KC783054	KC783003	KC783111	AF316495	KC783213	KC783253	—	AF411537	EF080809|	FJ155482

Downloaded from https://academic.oup.com/sysbio/article/63/4/582/1623176 by guest on 20 August 2022

branch lengths that was shorter than the MrBayes default (*prset Brlenspr = Unconstrained:Exp(100)*).

Comparisons between Phylogenies

We carried out simulations and implemented a likelihood approach to determine which morphological characters significantly supported incorrect nodes (Fig. 1, middle and lower right). Three nodes recovered in combined data analyses, deemed incorrect based on the molecular statistical scaffold and previously published molecular and morphological phylogenies (Simmons 1996; Baker et al. 2003; Datzmann et al. 2010; Dávalos et al. 2012), were used to develop this method. First, we calculated the per-character likelihoods of the morphological data given the scaffold tree, and given the same tree modified only to contain the incorrect node (Fig. 1, middle right). This was accomplished by using the computation of per-site log likelihoods and the Mkv+gamma model in RAxML (i.e., using the -f *g*, -z *file_with_trees*, -s *morphological_data*, and -K *MK* commands) (Stamatakis 2006). Then, null distributions of differences between the fit of characters to the tree with and without the incorrect node were generated for each of the 278 morphological characters. Morphological characters were simulated using the *rTraitDisc* function in the *ape* R package v.3.0-5 (Paradis et al. 2004). Simulating discrete characters requires a phylogeny with branch lengths and a transition matrix of rates of change between character states (Pagel 1994). The structure of each transition matrix assigned both the number of character states and whether or not the character was ordered. To facilitate simulation, transition matrices consisted only of 0/1 values. This meant that the branch lengths of each phylogeny used as simulation input had to be multiplied by the rate of character evolution so that the rate of change in the corresponding transition matrix equaled 1. The posterior distributions of Bayesian morphological phylogenies and evolutionary rate parameter (*m* in MrBayes) were used to generate these scaled phylogenies. Finally, the per-character log-likelihoods of simulated data sets were obtained using RAxML and the resulting distributions of differences in site likelihoods were used to determine which morphological characters were outliers in their support for particular nodes (Fig. 1, lower right).

RESULTS

Characteristics of the Morphological Data

The state: step plot showed the accumulation of character states slowed down as steps accumulated in the phylogeny (Fig. 2). The inflection point of the curve was estimated at 878 steps (standard error = 2.625). Steps in which a new character state was first observed occurred earlier in the phylogeny and were ranked lower than other steps ($W = 203{,}034$, P-value = 6.587E-05). The ordered-character relationship provided a substantially better fit to the data (AIC = 11,081) than the finite-state relationship (AIC = 18,662). Curves predicted using the fitted models are shown in Figure 2.

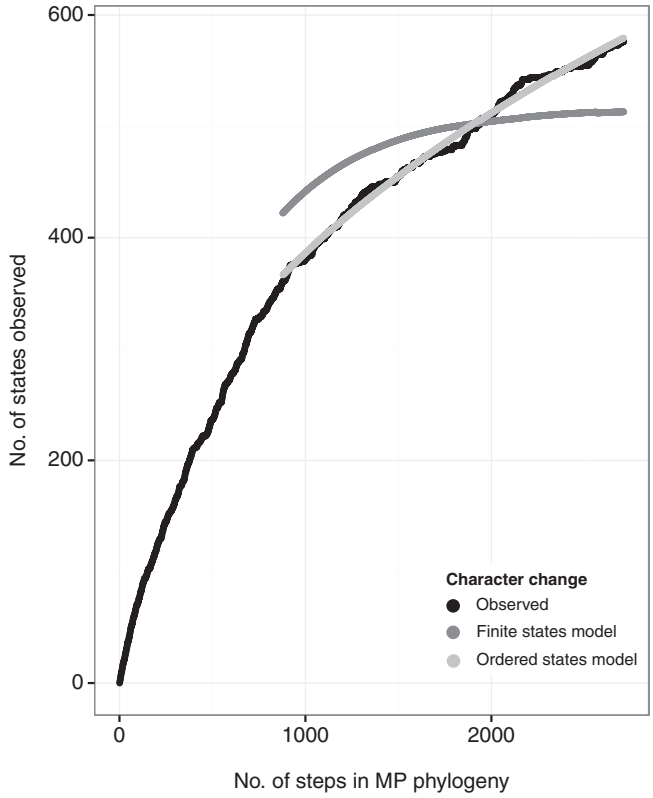

FIGURE 2. State: step plot for morphological data optimized using MP. Lines fitted using the finite-states (or rarefaction) and ordered-states (or hypervolume) models are shown for all points beyond the linear accumulation of character states.

The frequency distributions of pairwise dissimilarities from molecular and morphological data were markedly different (Fig. 3A). Relative distribution analyses revealed the greatest difference between morphological and molecular distributions consisted of an excess of very low dissimilarities, and lack of dissimilarities above 0.2 among morphological characters (Fig. 3B). Dental characters encoded variation similar to that in other morphological characters, whereas molecular characters encoded highly dissimilar variation in comparison. Phylogenetic analyses of the dental data resulted in weakly supported trees that were markedly different from previous morphological and molecular phylogenies (Supplementary Fig. S1). Optimal trees recovered using each approach were used in subsequent site-likelihood comparisons.

Phylogenetic Analyses

The optimal partition found using PartitionFinder had seven partitions: each of the three codon positions for the mitochondrial data, mt rRNA loops, mt rRNA stems, introns and the 3′ UTR, and protein-coding nuclear

Downloaded from https://academic.oup.com/sysbio/article/63/4/582/1623176 by guest on 20 August 2022

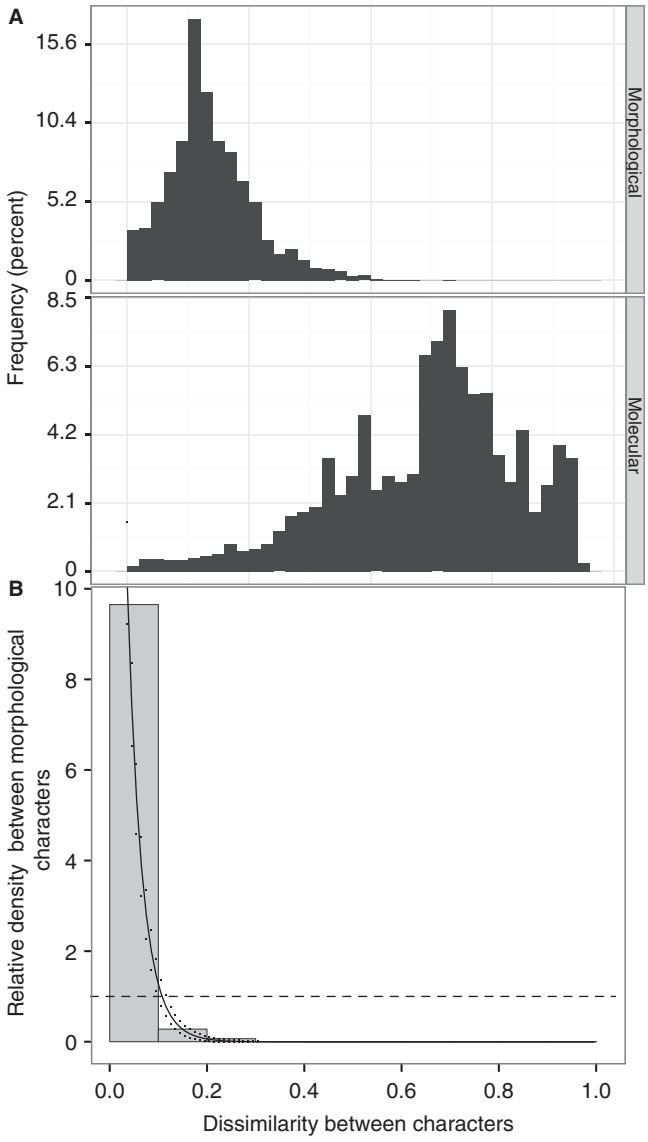

FIGURE 3. Frequency distributions and relative frequency distribution of Gower dissimilarities from molecular and morphological characters. (**A**) Frequency distributions of dissimilarity of morphological (upper) and molecular (lower) characters. (**B**) Frequency distribution of dissimilarities between morphological characters relative to dissimilarities between molecular characters. Solid bars show the observed relative density, and the solid black line shows the smoothed density of morphological character dissimilarities relative to the dissimilarity among variable molecular characters. The dashed black line indicates the expected relative density if the frequency distributions of dissimilarities from morphological and molecular data were not significantly different. Significant differences between frequency distributions occur in intervals above and below the dashed line.

sequences. The optimal model of sequence evolution for nuclear protein-coding genes, mitochondrial second and third codon positions, and mt rRNA loops was the GTR+gamma (Tavaré 1986; Yang 1994). For introns and the 3′ UTR, mitochondrial first positions and mt rRNA stems, the optimal model was the symmetrical (SYM)+gamma (Zharkikh 1994).

After discarding a burn-in of 1 million generations, Bayesian analyses of the molecular data using optimal partitions and models yielded a resolved and generally well-supported phylogeny (Supplementary Fig. S2). Examination of the posterior distribution of log-likelihoods and tree lengths showed that these parameters were autocorrelated up to every 7000 generations. The posterior distribution of trees was sampled every seven trees to obtain an uncorrelated posterior for subsequent analyses. A random sample of 1000 trees was used to constrain ML searches to generate the statistical scaffold. The resulting phylogeny reflected the phylogenetic uncertainty and support from both the Bayesian molecular posterior and the morphological ML searches (Fig. 4A). The placement of incomplete Miocene fossils received high support, corresponding to 99–100% of sampled trees.

Convergence in combined Bayesian analyses was achieved after 1 million generations, and the summary of multiple independent runs resulted in a well-resolved and weakly supported phylogeny (Fig. 4B). The relative levels of support were similar to those of the combined ML phylogeny (cf. Fig. 5A), with two important differences in resolution. The combined ML phylogeny, statistical scaffold, and morphological phylogenies placed the monotypic extant genus *Neonycteris* (known only from morphology) in a clade with *Trinycteris* (and, often, *Glyphonycteris* Figs. 4A and 5A and Supplementary Fig. S1). The combined ML phylogeny and statistical scaffold placed †*Palynephyllum* in a clade with *Platalina* and *Xeronycteris* (Figs. 4A and 5A). In contrast, the combined Bayesian phylogeny placed *Neonycteris* within *Micronycteris* with a posterior probability of 0.91, and †*Palynephyllum* in a clade of all nectar-feeding phyllostomids (Fig. 4B; Bayesian posterior probability = 0.91). The phylogenetic position of the two †*Notonycteris* species was unchanged in combined phylogenies relative to the statistical scaffold and was also supported in morphological phylogenies. ML analyses of the combined data resulted in a phylogeny similar to Bayesian analyses, crucially differing in placing *Lonchorhina* as sister to Phyllostominae (Fig. 5A).

Comparisons between Phylogenies

Three nodes highlighted in Figures 4B and 5A were identified as incorrect based on the statistical scaffold: (1) the node uniting all nectar-feeding phyllostomids (MRCA of *Lonchophylla* and *Glossophaga* in Fig. 4B), (2) *Lonchorhina* as sister to the subfamily Phyllostominae, and (3) *Neonycteris* nested within *Micronycteris*. The first two nodes have also been rejected in previous phyllostomid phylogenies generated using data included in our analyses (Baker et al. 2003; Dávalos et al. 2012), and a combination of overlapping and non-overlapping loci (Datzmann et al. 2010). No previous combined analysis has included *Neonycteris*, which is known only from the type series (Simmons 2005). Molecular data are not available for this monotypic

Downloaded from https://academic.oup.com/sysbio/article/63/4/582/1623176 by guest on 20 August 2022

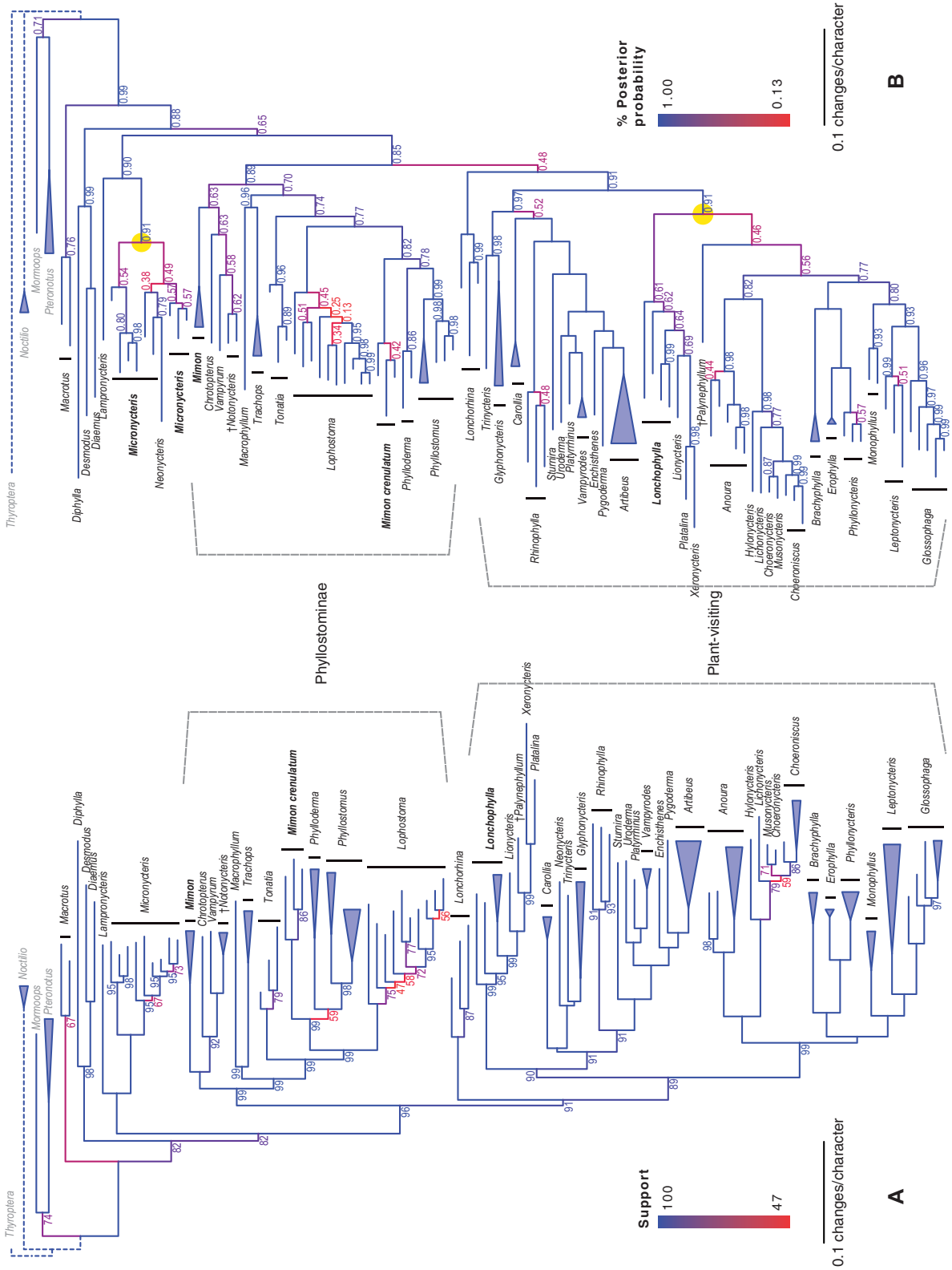

FIGURE 4. Summaries of statistical molecular scaffolds and combined Bayesian analyses. Branches collapsed into triangles had maximum support, † identifies fossil lineages, non-monophyletic genera are in bold and outgroups are in gray font. Subfamily Phyllostominae *sensu* Baker et al. (2003) is indicated. (**A**) Statistical scaffold phylogeny. Maximum clade credibility tree derived from ML analyses of morphological data constrained to each of 1000 uncorrelated Bayesian posterior molecular phylogenies. The mean of the log-likelihood of the data given the model was −119,913 (standard deviation = 107). Dashed line indicates branch is not shown to scale. Percent support values <100 are shown above or below internal branches, branch and number colors are scaled to support. (**B**) Combined Bayesian phylogeny. Consensus phylogram of all compatible bipartitions in Bayesian posterior trees from four independent runs (eight chains total) of Bayesian analyses of combined DNA sequence and morphological data. The harmonic mean of the posterior log-likelihood of the model given the data was −115,118. Percent Bayesian posterior probabilities <1.00 are shown below or above internal branches, branch and number colors are scaled to posterior probability. Highlighted nodes conflicted with the molecular phylogeny (and the statistical scaffold) and were further analyzed to identify morphological characters that strongly supported them (see Fig. 6).

Downloaded from https://academic.oup.com/sysbio/article/63/4/582/1623176 by guest on 20 August 2022

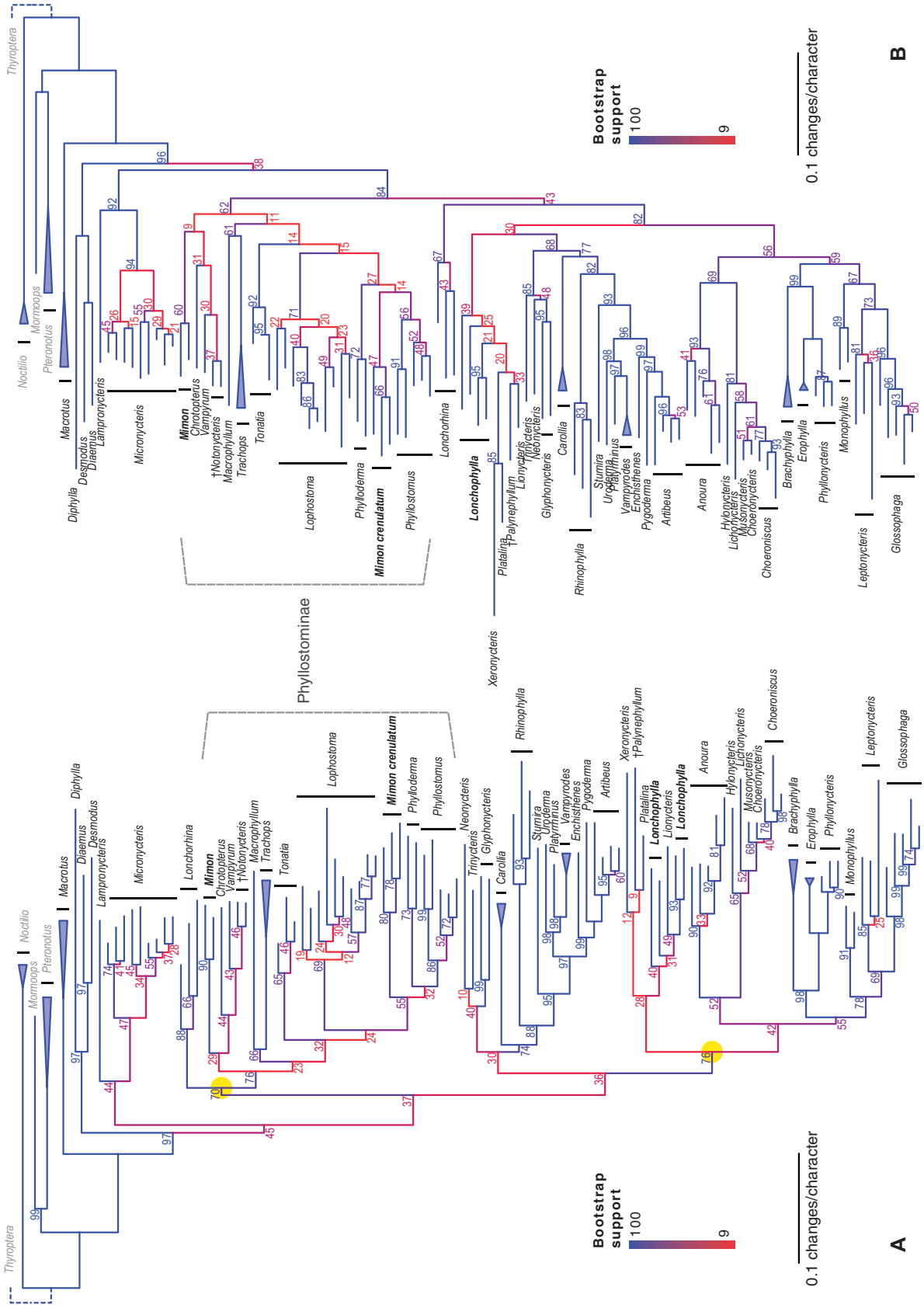

FIGURE 5. ML phylogenies resulting from analyses of combined DNA sequence and morphological data using RAxML. Branches collapsed into triangles had maximum support, † identifies fossil genera or species, non-monophyletic genera are in bold and outgroups are shown in gray font. Dashed line indicates branch is not shown to scale. Percent bootstrap values <100 are shown above or below internal branches, branch and number colors are scaled to bootstrap value. Subfamily Phyllostominae *sensu* Baker et al. (2003) is indicated. (**A**) ML phylogeny of combined data including all morphological characters (log-likelihood = −119,768). The highlighted node conflicted with the molecular phylogeny (and the statistical scaffold) and was further analyzed to identify morphological characters that strongly supported it (see Fig. 6). (**B**) ML phylogeny of partitioned DNA sequence data, and morphological data excluding 32 morphological characters (Supplementary Table S6; log-likelihood = −117,270).

Downloaded from https://academic.oup.com/sysbio/article/63/4/582/1623176 by guest on 20 August 2022

genus. Both previous morphological analyses and ML analyses of combined data (Fig. 5A) suggest that *Neonycteris* is more closely related to *Trinycteris* and *Glyphonycteris* than to *Micronycteris* (Simmons 1996).

The log-likelihood of character node support was compared with the null distribution of per-character difference in log-likelihood. The distribution of support or rejection for incorrect nodes from individual dental characters is shown in Figure 6. The three nodes received different levels of support from the morphological data, with overwhelmingly more outliers supporting than rejecting the monophyly of nectar-feeding phyllostomids (10:1), fewer outliers supporting than rejecting *Lonchorhina* as sister to the Phyllostominae, and 10 outliers supporting and five rejecting the inclusion of *Neonycteris* in *Micronycteris* (13:14; Fig. 5).

Thirty-two significant positive outliers (one character overlapped in support for two nodes) were then excluded from the combined data matrix (Supplementary Table S6). The resulting phylogeny was generally weakly supported, especially within the subfamily Phyllostominae and between *Lonchophylla* and its relatives (Fig. 5B). However, support values across nodes from analyses of the trimmed data set were often *higher* than those from analyses including all the data (Fig. 5B). The position of †*Palynephyllum* was equivalent to that found in the statistical scaffold (i.e., within the crown Lonchophyllinae *sensu* Baker et al. 2003) and †*Notonycteris* remained sister to *Vampyrum* (Fig. 5B).

Discussion

Integrating Morphological and Molecular Data

We propose new methods to integrate morphological and molecular characters that more rigorously address conflict caused by morphological homoplasy. In a previous contribution (Dávalos et al. 2012), we examined saturation in both morphological and molecular character states and applied likelihood approaches to identify strongly conflicting molecular characters. Here, we focus on diagnosing homoplasy in morphological data, and implementing new methods to isolate significantly conflicting signal and integrate morphological and molecular characters. These new methods were applied to an empirical data set to place the Miocene fossils in the phylogeny of New World leaf-nosed bats and understand the evolutionary history of the family. Instead of either automatically constraining the signal from morphological data to conform to a single molecular scaffold (Springer et al. 2001), or unconditionally combining the data (Hermsen and Hendricks 2008), we aimed to uncover evidence of homoplasy in morphological data, and identify and exclude characters involved in conflicts arising from homoplasy (Wiens et al. 2003; Dávalos et al. 2012). To accomplish these objectives, we explored the patterns of variation in morphological data, extended molecular scaffolds to account for variation

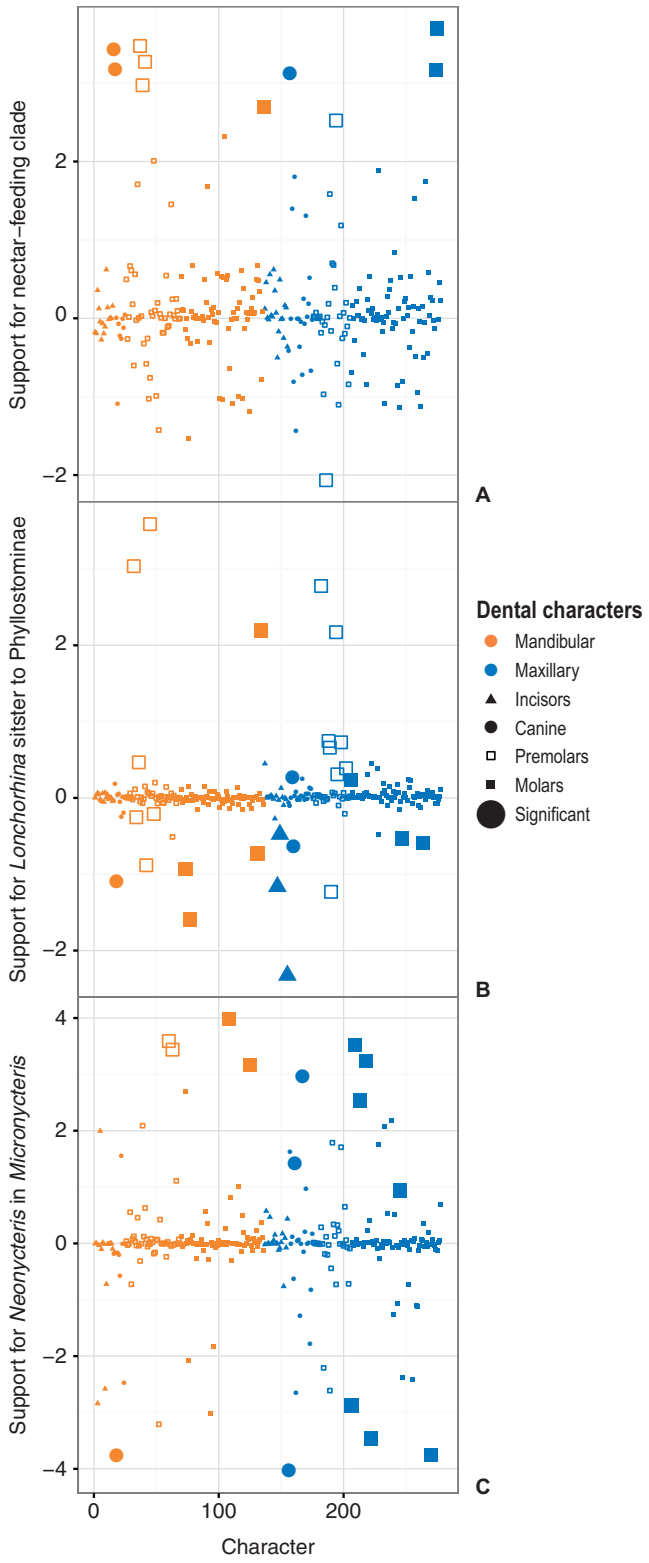

FIGURE 6. Observed differences in morphological per-character log-likelihood between trees containing the clades and the statistical scaffold tree. Values above the 0 line indicate support, below indicate rejection. Large symbols indicate statistically significant outliers. (**A**) Morphological support or rejection for a clade of nectar-feeding phyllostomids. (**B**) Morphological support or rejection for a clade of *Lonchorhina* and Phyllostominae. (**C**) Morphological support or rejection for *Neonycteris* nesting within *Micronycteris*.

Downloaded from https://academic.oup.com/sysbio/article/63/4/582/1623176 by guest on 20 August 2022

in phylogenies estimated from DNA sequences, and introduced a site-likelihood approach to identify characters supporting particular nodes. These methods respond to a major challenge in phylogenetics: how to integrate morphological and molecular data and estimate relationships between fossil and extant taxa (Manos et al. 2007; Wiens 2009).

Molecular scaffolds and combined data analyses reflect two divergent views on integrating morphological data in phylogenetic analyses. Scaffolds were originally introduced to overcome two analytical challenges in optimizing morphological and molecular data: the use of MP and the lack of molecular data for extinct taxa (Springer et al. 2001). Since then, models of morphological evolution have been proposed, ML and Bayesian methods to analyze combined data have been implemented (Lewis 2001; Ronquist and Huelsenbeck 2003), and the impact of missing data on phylogenies has been found to be small (Wiens and Moen 2008; Smith et al. 2009; Wiens 2009; Wiens and Tiu 2012). Instead, biological drivers of homoplasy, including ecological convergence and correlations among character states arising through development (Kangas et al. 2004; Evans et al. 2007; Dávalos et al. 2012), have emerged as the main reasons to use scaffolds (Springer et al. 2007; 2008).

The alternative to scaffolds is combining and simultaneously analyzing morphological and molecular data on equal footing (Hermsen and Hendricks 2008). The most compelling argument for using all available data (or the total evidence) is that all phylogenetically informative characters should be used in estimating phylogenies. In the absence of systematic error and if each character provides independent evidence for relationships, combining all the data will then provide the most powerful inference of phylogeny (de Queiroz and Gatesy 2007). The profusion of genomic data has revealed that systematic error from mutational bias can be common (Phillips et al. 2004; Baurain et al. 2007; Dávalos and Perkins 2008), and natural selection can generate significant support for incorrect relationships (Castoe et al. 2009; Li et al. 2010; Liu et al. 2010; Davies et al. 2012). Constraints imposed by the genetic code, molecular interactions, selection, and developmental processes imply that many molecular and morphological characters are not independent (Emerson and Hastings 1998; O'Keefe and Wagner 2001; Carrier et al. 2005; Skelly et al. 2013). Critically, models that account for various sources of systematic error with molecular sequences are available and can be deployed when saturation or mutational biases are suspected (Muse and Gaut 1994; Schöniger and Von Haeseler 1994; Gruber et al. 2007; Blanquart and Lartillot 2008). Comparisons between loci make the detection of convergence shaped by adaptation possible with genetic data (Castoe et al. 2009; Li et al. 2010; Liu et al. 2010; Dávalos et al. 2012; Davies et al. 2012).

Models of morphological evolution have been slower to develop, as states across different morphological characters are fundamentally incomparable, an obstacle that is largely absent for molecular characters. The most widely applied model (Mkv), for example, is an extension of the Jukes-Cantor model first published in 1969 (Jukes and Cantor 1969). Under these circumstances, methods that analyze the accumulation of homoplasy and correlated evolution in morphological characters can be helpful in deciding whether systematic error is present, or if the assumption of independence is warranted (Emerson and Hastings 1998; Wagner 2000; O'Keefe and Wagner 2001). Detecting and correcting for the consequences of ecological convergence driven by morphological adaptation is more difficult because it requires comparisons to independent phylogenies (Wiens et al. 2003; Holland et al. 2010). Either way, investigating the data structure and phylogenetic signal of morphological characters can help illuminate the biological processes that shape phenotypic variation (Dávalos et al. 2012).

As in previous analyses of the phylogeny of extant mammals (Springer et al. 2007; 2008; Lee and Camens 2009), morphological characters rejected relationships estimated with multiple loci (Supplementary Fig. S1). Based on their results, Springer et al. (2007) concluded that homology and homoplasy were confounded in morphological characters, with homoplasy prevailing, and cautioned the need to reexamine both character coding and models of morphological evolution. Hermsen and Hendricks (2008) and Asher et al. (2008) have nonetheless argued for combining data because the evidence of morphological homoplasy arose through incongruence with molecular phylogenies, and incongruence may also be observed among different genes. The data structure of our new morphological characters, however, revealed the randomization of phylogenetic signal and the potential for amplification of homoplasy before any comparisons with molecular phylogenies were undertaken.

Just as the randomization of phylogenetic signal can be assessed in molecular data by examining the saturation of changes through time, the plateauing of new character states relative to changes in the phylogeny or character exhaustion indicates homoplasy in morphological data (Wagner 2000). The pattern of character state changes found in the dental character data in phyllostomids indicates saturation (Fig. 2). Another indication of saturation in molecular data is a high rate of change inferred using model-based methods. We compared the relative rates of change estimated for each of the partitions in Bayesian combined analyses (m_i parameters in MrBayes output) to compare the morphological rate of change to molecular substitution rates. With a median rate of 2.9 substitutions/character, the relative rate of change for the morphological partition was the second highest observed. Only mitochondrial third codon positions had higher rates of change (median = 7.2 substitutions/site), and morphological rates of change were consistently at least one order of magnitude higher than all nuclear partitions and most mitochondrial data (Table 2). Both saturation and high rates of change indicate homoplasy is present in the morphological data.

Downloaded from https://academic.oup.com/sysbio/article/63/4/582/1623176 by guest on 20 August 2022

TABLE 2. Posterior estimates of relative rates of change from non-clock combined Bayesian analysis of combined data, ranked from fastest to slowest

Partition	Median	95% HPD lower	95% HPD upper
Mt pos. 3	7.244	6.710	7.801
Morphology	2.889	2.553	3.240
Mt rRNA loops	1.875	1.718	2.033
Mt pos. 1	0.478	0.429	0.533
Mt rRNA stems	0.364	0.327	0.403
Introns	0.263	0.241	0.285
Mt pos. 2	0.128	0.101	0.160
Nuclear	0.118	0.108	0.128

Notes: Rates are in substitutions/site for molecular data and changes/character for morphology. HPD = high probability density, mt = mitochondrial, pos. = position, rRNA = ribosomal RNA.

High rates of change alone cannot explain how saturation in morphological changes affected the combined phylogeny. If changes from one character state to another were random relative to common descent, and independent from one another, then resulting trees should be unresolved or weakly supported. Strongly supported conflicts must arise through additional processes besides high rates of change. One of the nodes uncovered in combined analyses and identified as conflicting with prior hypotheses was strongly supported (Bayesian posterior probability >0.90 in Fig. 4B and ML bootstrap >75% in Fig. 5A). Evolutionary processes that superimposed on saturated changes result in strong homoplasious signal have been extensively studied in molecular data (Phillips et al. 2004). In some lineages, for example, mutational biases toward AT at 4-fold degenerate positions produce significantly conflicting signal at saturated sites (Gruber et al. 2007; Dávalos and Perkins 2008). This process generates character states that are both homoplastic and correlated, as all sites throughout the genome experience similar mutational bias and end up having similar character states.

One consequence of proposed functional and developmental constraints on the phenotype is the non-independence of morphological character states. As expected if functional and developmental processes operated simultaneously on multiple aspects of morphology, dental characters were much more similar to one another than molecular characters (Fig. 3). These analyses were not meant to infer particular associations between character states. There are hypothesis-testing approaches to infer such associations (Huelsenbeck et al. 2003; Pagel and Meade 2006), but these were not designed to conduct all possible pairwise comparisons (Bollback 2006). The dissimilarity analyses do suggest pervasive non-independence in morphological characters and, together with the saturation of character state changes, have implications for integrating morphology in phylogenetic analyses.

The morphological characters employed in this study were saturated and recurrently encoded similar patterns of variation, indicating direct unweighted analyses of these data would be inappropriate. The frequency distribution of morphological dissimilarities suggests that new models of evolution will need to account for non-independence between morphological characters. For molecular data, such models (e.g., doublet and codon models) are computationally intensive and known biochemical properties of nucleotides and proteins help define and estimate parameters of correlated evolution (Muse and Gaut 1994; Schöniger and Von Haeseler 1994). The processes that generate correlations among morphological traits are understood best for mammalian teeth and angiosperm leaves, and these might be the best targets for developing and testing more complex models (Kangas et al. 2004; Geeta et al. 2012). Finally, the assumption of independence among characters that underlies the key argument for total evidence is violated to a greater extent with morphological than with molecular data. These findings warrant close examination of the morphological characters to better account for their combination of phylogenetic and homoplasious saturated signal.

We introduced a new method to identify strongly conflicting morphological characters and reduce the impact of homoplasy on combined phylogenetic analyses. Unfortunately, the characters supporting those nodes could not have been identified *a priori*. For example, nectar feeding in phyllostomids is associated with modifications to the incisors (Carstens et al. 2002), but none of the characters supporting the nectar-feeding clade involved the incisors (Fig. 6A). In a precedent for these results, Carstens et al. (2002) found no significant conflict between the phylogenetic signals from incisor, hyoid, and tongue characters involved in nectarivory and signal from other morphological characters. Upper and lower dentition characters, mostly from the premolars and molars, supported the other two nodes. Despite the focus on only three nodes, excluding a subset of characters *a posteriori* reduced the number of strongly supported conflicts across the entire phylogeny (Supplementary Table S6, cf. Fig. 4A and 5).

Instead of providing the most powerful phylogenetic hypothesis, our results suggest that combined analyses may reflect homoplasy in the morphological data. Given the saturation, high rates of evolution, non-independence, conflicting signal, and inadequacy of current models of evolution for inferring phylogeny from dental characters, the statistical scaffold summarizes the phylogenies that best capture phylogenetic signal in the data (Fig. 4A).

Phylogeny of Miocene Phyllostomidae

We undertook the first family-wide analyses of Miocene fossil phylogeny. The integrative phylogenies analyzed here confirmed the close relationship between the two †*Notonycteris* species and the carnivorous genera *Vampyrum* and *Chrotopterus* (Czaplewski et al. 2003b) (Figs. 4 and 5). Since its original description, †*Palynephyllum* has been hypothesized to be a nectar-feeding lineage based on its morphology (Czaplewski

Downloaded from https://academic.oup.com/sysbio/article/63/4/582/1623176 by guest on 20 August 2022

et al. 2003b). That hypothesis was supported in all phylogenetic analyses (Figs. 4 and 5). The resolution varied between †*Palynephyllum* being nested within a spurious nectar-feeding clade in combined Bayesian analyses (Fig. 4B), or nesting among the lonchophyllines *Platalina*, *Xeronycteris*, and *Lionycteris* (Figs. 4A and 5). The first resolution is equivalent to the dating constraint imposed in several previous dating analyses for phyllostomids (Baker et al. 2010; Dávalos 2010; Rojas et al. 2011; Dumont et al. 2012), while the second is unprecedented and may change ingroup divergence dates. The difficulties with integrating morphological characters in phylogenetic analyses and fragmentary nature of the †*Palynephyllum* remains suggest caution in concluding that this fossil is a crown lonchophylline. An independent line of evidence—biogeography—supports the latter conclusion.

Biogeography of †Palynephyllum.—In glossophagines, known diversification events among genera are exclusively restricted to Mesoamerica and the West Indies (Dávalos 2010; Rojas et al. 2012). In contrast, both generic and species-level diversity of lonchophyllines is concentrated in South America (Gregorin and Ditchfield 2005; Mantilla-Meluk 2007). In the Miocene, the La Venta site was isolated from Mesoamerica and interconnected to South America (Hoorn et al. 1995). A phylogenetic placement of the fossil †*Palynephyllum* as a stem glossophagine or a stem plant-visiting phyllostomid would imply that, outside the genus *Anoura*, glossophagines either failed to diversify on the South Americas continent or did diversify and then went extinct. These hypotheses are both plausible, but require additional explanations. †*Palynephyllum* traces the evolutionary history of the lonchophyllines to South America, where all known diversification events in that clade have unfolded and is thus consistent with both the paleogeography of the region and the biogeography of diversification in nectar-feeding phyllostomids.

Conclusions

By investigating the rates of evolution and quantifying the similarity between dental characters scored in phyllostomid bats and their relatives, we demonstrate that these morphological data show saturation and non-independence. We introduce two approaches to compensate for these model violations, one extending molecular scaffolds to posterior series of trees in a likelihood framework, and the other identifying strongly conflicting characters for subsequent character analyses. Applying these new methods to analyses integrating molecular and morphological data, we confirm close relationships among the extant carnivorous genera *Chrotopterous* and *Vampyrum*, and †*Notonycteris*; and support the novel conclusion that †*Palynephyllum* is a member of the nectarivorus crown Lonchophyllinae. Both fossils trace the history of their clades to the middle Miocene of northern South America. By quantifying homoplasious signal and similarities, and identifying strongly conflicting characters, the approaches we developed here are one step toward future methods to model the evolution of saturated and correlated morphological characters.

Supplementary Material

Data available from the Dryad Digital Repository: http://dx.doi.org/10.5061/dryad.pg4c0.

Funding

The National Science Foundation (DEB-0949759 to L.M.D. and DEB-0949859 to N.B.S.).

Acknowledgments

We thank Noa Krawczyk, James Proffitt, Dani Saks, and Susan Tsang for collection of morphological data, and the NSF Research Experience for Undergraduates (REU) program at the AMNH for supporting Saks, Krawczyk, and Proffitt. This work would have been impossible without the work of collectors and the infrastructure provided by natural history collections. For access to morphological specimens we thank the staff at the Mammalogy Department of the American Museum of Natural History (AMNH); the Field Museum of Natural History (FMNH); the Florida Museum of Natural History (FLMNH); the Instituto de Ciencias Naturales (ICN. Bogotá, Colombia); the Instituto Nacional de Investigaciones Geológico-Mineras (IGM, Bogota, Colombia); the Museo de Historia Natural, Universidad Nacional Mayor de San Marcos (MUSM, Lima, Peru); the Museum of Vertebrate Zoology at the University of California, Berkeley (MVZ); the Royal Ontario Museum (ROM); the Natural Science Research Laboratory at Texas Tech University (TTU); Bill Clemens at the University of California Museum of Paleontology (UCMP); and Kris Helgen at the Smithsonian Institution (USNM). For tissue loans, we thank the staff at the Ambrose Monell Cryo-Collection at AMNH, and Bruce Patterson and John D. Phelps at the FMNH. For great ideas and editing for Figure 1, we thank Romain Dahan, Samantha DelSerra, Jacob Roday, Danny Rojas, Laurel R. Yohe, and Xiaoyu Zhang. We thank Nicole M. Gerardo for finding a way to render morphological character states comparable. Part of this work was performed on the Abel Cluster, owned by the University of Oslo and the Norwegian metacenter for High Performance Computing (NOTUR), and operated by the Research Computing Services group at USIT, the University of Oslo IT department.

References

Alheit K., Reif J., Maurer H., Hahn V., Weissmann E., Miedaner T., Wurschum T. 2011. Detection of segregation distortion loci in triticale (x *Triticosecale* Wittmack) based on a high-density DArT marker consensus genetic linkage map. BMC Genomics 12:380.

Downloaded from https://academic.oup.com/sysbio/article/63/4/582/1623176 by guest on 20 August 2022

Asher R.J., Geisler J.H., Sánchez-Villagra M.R. 2008. Morphology, paleontology, and placental mammal phylogeny. Syst. Biol. 57:311–317.

Baker R.J., Bininda-Emonds O.R.P., Mantilla-Meluk H., Porter C.A., Van Den Bussche R. 2010. Molecular timescale of diversification of feeding strategy and morphology in New World leaf-nosed bats (Phyllostomidae): a phylogenetic perspective. In: Gunnell G.F., Simmons N.B., editors. Evolutionary History of Bats: Fossils, Molecules and Morphology. Cambridge (MA): Cambridge University Press.

Baker R.J. Porter C.A., Hoofer S.R., Van Den Bussche R.A. 2003. Diversification among New World Leaf-Nosed bats: an evolutionary hypothesis and classification inferred from digenomic congruence of DNA sequence. Occasional Papers, Museum of Texas Tech University 230:1–32.

Baker R.J., Porter C.A., Patton J.C., Van Den Bussche R.A. 2000. Systematics of bats of the family Phyllostomidae based on *RAG*2 DNA sequences. Occasional Papers, Museum of Texas Tech University 202:1–16.

Baurain D., Brinkmann H., Philippe H. 2007. Lack of resolution in the animal phylogeny: closely spaced cladogeneses or undetected systematic errors? Mol. Biol. Evol. 24:6–9.

Bininda-Emonds O.R.P. 2005. transAlign: using amino acids to facilitate the multiple alignment of protein-coding DNA sequences. BMC Bioinform. 6:156.

Blanquart S., Lartillot N. 2008. A site- and time-heterogeneous model of amino-acid replacement. Mol. Biol. Evol. 25:842–858.

Bollback J.P. 2006. SIMMAP: stochastic character mapping of discrete traits on phylogenies. BMC Bioinform. 7:88.

Burnham K.P., Anderson D.R. 2002. Model selection and multimodel inference. New York: Springer-Verlag.

Carrier D.R., Chase K., Lark K.G. 2005. Genetics of canid skeletal variation: size and shape of the pelvis. Genome Res. 15: 1825–1830.

Carstens B.C., Lundrigan B.L., Myers P. 2002. A phylogeny of the neotropical nectar-feeding bats (Chiroptera: Phyllostomidae) based on morphological and molecular data. J. Mamm. Evol. 9:23–53.

Castoe T.A., de Koning A.P.J., Kim H.-M., Gu W., Noonan B.P., Naylor G., Jiang Z.J., Parkinson C.L., Pollock D.D. 2009. Evidence for an ancient adaptive episode of convergent molecular evolution. Proc. Natl Acad. Sci. USA 106:8986–8991.

Choate J.R., Birney E.C. 1968. Sub-recent Insectivora and Chiroptera from Puerto Rico, with the description of a new bat of the genus *Stenoderma*. J. Mammal. 49:400–412.

Clare E.L., Lim B.K., Engstrom M.D., Eger J.L., Hebert P.D.N. 2007. DNA barcoding of Neotropical bats: species identification and discovery within Guyana. Mol. Ecol. Notes 7:184–90.

Clare E.L., Lim B.K., Fenton M.B., Hebert P.D.N. 2011. Neotropical bats: estimating species diversity with DNA barcodes. PLoS One 6:e22648.

Czaplewski N.J., Krejca J., Miller T.E. 2003a. Late quaternary bats from Cebada Cave, Chiquibul Cave System, Belize. Caribb. J. Sci. 39:23–33.

Czaplewski N.J., Takai M., Naeher T.M., Shigehara N., Setoguchi T. 2003b. Additional bats from the middle Miocene La Venta fauna of Colombia. Revista de la Academia Colombiana de Ciencias Físicas, Exactas y Naturales 27:263–282.

Datzmann T., von Helversen O., Mayer F. 2010. Evolution of nectarivory in phyllostomid bats (Phyllostomidae Gray, 1825, Chiroptera: Mammalia). BMC Evol. Biol. 10:165.

Dávalos L.M. 2010. Earth history and the evolution of Caribbean bats. In: Fleming T.H., Racey P.A., editors. Island bats: ecology, evolution, and conservation. Chicago (IL): University of Chicago Press. p. 96–115.

Dávalos L.M., Cirranello A.L., Geisler J.H., Simmons N.B. 2012. Understanding phylogenetic incongruence: lessons from Phyllostomid bats. Biol. Rev. 87:991–1023.

Dávalos L.M., Perkins S.L. 2008. Saturation and base composition bias explain phylogenomic conflict in *Plasmodium*. Genomics 91:433–442.

Dávalos L.M., Russell A.L. 2012. Deglaciation explains bat extinction in the Caribbean. Ecol. Evol. 2:1–7.

Dávalos L.M., Turvey S. 2012. West Indian mammals: the old, the new, and the recently extinct. In: Patterson B.D., Acosta L.P., editors. Bones, clones, and biomes: an extended history of recent neotropical mammals. Chicago (IL): University of Chicago Press, p. 157–202.

Davies K.T.J., Cotton J.A., Kirwan J.D., Teeling E.C., Rossiter S.J. 2012. Parallel signatures of sequence evolution among hearing genes in echolocating mammals: an emerging model of genetic convergence. Heredity 108:480–489.

Davis B.H., Poon A.F.Y., Whitlock M.C. 2009. Compensatory mutations are repeatable and clustered within proteins. Proc. R. Soc. B 276:1823–1827.

de Queiroz A., Gatesy J. 2007. The supermatrix approach to systematics. Trends Ecol. Evol. 22:34–41.

Drummond A.J., Ashton B., Buxton S., Cheung M., Cooper A., Duran C., Field M., Heled J., Kearse M., Markowitz S., Moir R., Stones-Havas S., Sturrock S., Thierer T., Wilson A. 2011. Geneious. Geneious version 5.3.6. Available from http://www.geneious.com/.

Dumont E.R., Dávalos L.M., Goldberg A., Voigt C.C., Rex K., Santana S.E. 2012. Morphological innovation, diversification and the invasion of a new adaptive zone. Proc. R. Soc. B 279: 1797–1805.

Eick G.N., Jacobs D.S., Matthee C.A. 2005. A nuclear DNA phylogenetic perspective on the evolution of echolocation and historical biogeography of extant bats (Chiroptera). Mol. Biol. Evol. 22: 1869–1886.

Emerson S.B., Hastings P.A. 1998. Morphological correlations in evolution: consequences for phylogenetic analysis. Q Rev Biol 73:141–162.

Evans A.R., Wilson G.P., Fortelius M., Jernvall J. 2007. High-level similarity of dentitions in carnivorans and rodents. Nature 445: 78–81.

Fracasso M.P.D.A., Salles L.D.O. 2005. Diversity of quaternary bats from Serra da Mesa (State of Goiás, Brazil). Zootaxa 817:1–19.

Geeta R., Dávalos L.M., Levy A., Bohs L., Lavin M., Mummenhoff K., Sinha N., Wojciechowski M. F. 2012. Keeping it simple: flowering plants tend to retain, and revert to, simple leaves. New Phytol. 193:481–493.

Gower J.C. 1966. Some distance properties of latent root and vector methods used in multivariate analysis. Biometrika 53:325–338.

Gregorin R., Ditchfield D.A. 2005. New genus and species of nectar-feeding bat in the tribe Lonchophyllini (Phyllostomidae: Glossophaginae) from northeastern Brazil. J. Mammal. 86:403–414.

Gruber K., Voss R., Jansa S. 2007. Base-compositional heterogeneity in the RAG1 locus among didelphid marsupials: implications for phylogenetic inference and the evolution of GC content. Syst. Biol. 56:83–96.

Gu X., Fu Y.X., Li W.H. 1995. Maximum likelihood estimation of the heterogeneity of substitution rate among nucleotide sites. Mol. Biol. Evol. 12:546–57.

Guindon S., Dufayard J.-F., Lefort V., Anisimova M., Hordijk W., Gascuel O. 2010. New Algorithms and methods to estimate maximum-likelihood phylogenies: assessing the performance of PhyML 3.0. Syst. Biol. 59:307–21.

Handcock M.S. 2013. reldist: relative distribution methods. R package. Available from http://www.stat.ucla.edu/~handcock/RelDist/.

Handcock M.S., Morris M. 1999. Relative distribution methods in the social sciences. New York: Springer.

Hermsen E.J., Hendricks J.R. 2008. W(h)ither fossils? Studying morphological character evolution in the age of molecular sequences. Ann. Mo. Bot. Gard. 95:72–100.

Holland B.R., Spencer H.G., Worthy T.H., Kennedy M. 2010. Identifying cliques of convergent characters: concerted evolution in the cormorants and shags. Syst. Biol. 59:433–445.

Hoorn C., Guerrero J., Sarmiento G.A., Lorente M.A. 1995. Andean tectonics as a cause for changing drainage patterns in Miocene northern South America. Geology 23:237–240.

Huelsenbeck J.P., Nielsen R., Bollback J.P. 2003. Stochastic mapping of morphological characters. Syst. Biol. 52:131–158.

Jansa S.A., Goodman S.M., Tucker P.K. 1999. Molecular phylogeny and biogeography of the native rodents of Madagascar (Muridae: Nesomyinae): a test of the single-origin hypothesis. Cladistics 15:253–270.

Downloaded from https://academic.oup.com/sysbio/article/63/4/582/1623176 by guest on 20 August 2022

Jukes T.H., Cantor C.R. 1969. Evolution of protein molecules. In: Munro H.N., editor. Mammalian protein metabolism. New York: Academic Press. p. 21–132.
Kangas A.T., Evans A.R., Thesleff I., Jernvall J. 2004. Nonindependence of mammalian dental characters. Nature 432:211–214.
Katoh K., Kuma K.-I., Toh H., Miyata T. 2005. MAFFT version 5: improvement in accuracy of multiple sequence alignment. Nucleic Acids Res. 33:511–518.
Katoh K., Toh H. 2008. Recent developments in the MAFFT multiple sequence alignment program. Brief. Bioinform. 9:286–298.
Lanfear R., Calcott B., Ho S.Y.W., Guindon S. 2012. PartitionFinder: combined selection of partitioning schemes and substitution models for phylogenetic analyses. Mol. Biol. Evol. 29:1695–1701.
Lee M.S.Y., Camens A.B. 2009. Strong morphological support for the molecular evolutionary tree of placental mammals. J. Evol. Biol. 22:2243–2257.
Legendre P., Gallagher E. 2001. Ecologically meaningful transformations for ordination of species data. Oecologia 129:271–280.
Lewis P.O. 2001. A likelihood approach to estimating phylogeny from discrete morphological character data. Syst. Biol. 50:913–925.
Li G., Wang J., Rossiter S.J., Jones G., Cotton J.A., Zhang S. 2008. The hearing gene *Prestin* reunites echolocating bats. Proc. Natl Acad. Sci. USA 105:13959–13964.
Li Y., Liu Z., Shi P., Zhang J. 2010. The hearing gene *Prestin* unites echolocating bats and whales. Curr. Biol. 20:R55–R56.
Liu Y., Cotton J.A., Shen B., Han X., Rossiter S.J., Zhang S. 2010. Convergent sequence evolution between echolocating bats and dolphins. Curr. Biol. 20:R53–R54.
Maechler M., Rousseeuw P., Struyf A., Hubert M., Hornik K. 2012. cluster: cluster analysis basics and extensions. R package version 1.15.2.
Manos P.S., Soltis P.S., Soltis D.E., Manchester S.R., Oh S.-H., Bell C.D., Dilcher D.L., Stone D.E. 2007. Phylogeny of extant and fossil juglandaceae inferred from the integration of molecular and morphological data sets. Syst. Biol. 56:412–430.
Mantilla-Meluk H. 2007. Lonchophyllini, the Chocoan bats. Revista Institucional Universidad Tecnológica del Chocó 26:49–57.
Marengo E., Robotti E., Gianotti V., Righetti P.G., Cecconi D., Domenici E. 2003. A new integrated statistical approach to the diagnostic use of two-dimensional maps. Electrophoresis 24:225–236.
Miller M.A., Pfeiffer W., Schwartz T. 2010. Creating the CIPRES science gateway for inference of large phylogenetic trees. Gateway Computing Environments Workshop (GCE), 2010. p. 1–8.
Muggeo V.M.R. 2008. Segmented: an R package to fit regression models with broken-line relationships. R News 8:20–25.
Murphy W.J., O'Brien S.J. 2007. Designing and optimizing comparative anchor primers for comparative gene mapping and phylogenetic inference. Nat. Protoc. 2:3022–3030.
Muse S.V., Gaut B.S. 1994. A likelihood approach for comparing synonymous and nonsynonymous nucleotide substitution rates, with application to the chloroplast genome. Mol. Biol. Evol. 11: 715–24.
O'Keefe FR, Wagner P.J. 2001. Inferring and testing hypotheses of cladistic character dependence by using character compatibility. Syst. Biol. 50:657–675.
O'Leary M.A., Kaufman S.G. 2012. MorphoBank 3.0: Web application for morphological phylogenetics and taxonomy. Available from http://morphobank.org.
Pagel M. 1994. Detecting correlated evolution on phylogenies: a general method for the comparative analysis of discrete characters. Proc. R. Soc. B 255:37–45.
Pagel M., Meade A. 2006. Bayesian analysis of correlated evolution of discrete characters by reversible-jump Markov Chain Monte Carlo. Am. Nat. 167:808–825.
Paradis E., Claude J., Strimmer K. 2004. APE: analyses of phylogenetics and evolution in R language. Bioinformatics 20:289–290.
Peterson L.E. 2003. Partitioning large-sample microarray-based gene expression profiles using principal components analysis. Comput. Methods Programs Biomed. 70:107–119.
Phillips M.J., Delsuc F., Penny D. 2004. Genome-scale phylogeny and the detection of systematic biases. Mol. Biol. Evol. 21:1455–1458.
Pyron R.A. 2011. Divergence time estimation using fossils as terminal taxa and the origins of Lissamphibia. Syst. Biol. 60:466–480.
R Development Core Team. 2012. R: a language and environment for statistical computing. Vienna, Austria: R Foundation for Statistical Computing.
Rambaut A., Drummond A.J. 2007. Tracer. Available from http://beast.bio.ed.ac.uk/Tracer.
Rambaut A., Drummond A.J. 2010. TreeAnnotator: MCMC Output analysis. Available from http://beast.bio.ed.ac.uk.
Rojas D., Vale Á., Ferrero V., Navarro L. 2011. When did plants become important to leaf-nosed bats? Diversification of feeding habits in the family Phyllostomidae. Mol. Ecol. 20:2217–2228.
Rojas D., Vale Á., Ferrero V., Navarro L. 2012. The role of frugivory in the diversification of bats in the Neotropics. J. Biogeogr. 39: 1948–1960.
Ronquist F., Huelsenbeck J.P. 2003. MrBayes 3: Bayesian phylogenetic inference under mixed models. Bioinformatics 19:1572–1574.
Ronquist F., Klopfstein S., Vilhelmsen L., Schulmeister S., Murray D.L., Rasnitsyn A.P. 2012a. A total-evidence approach to dating with fossils, applied to the early radiation of the Hymenoptera. Syst. Biol. 61:973–999.
Ronquist F., Teslenko M., van der Mark P., Ayres D.L., Darling A., Höhna S., Larget B., Liu L., Suchard M.A., Huelsenbeck J.P. 2012b. MrBayes 3.2: Efficient Bayesian phylogenetic inference and model choice across a large model space. Syst. Biol. 61:539–542.
Santana S.E., Geipel I., Dumont E.R., Kalka M.B., Kalko E.K.V. 2011. All you can eat: high performance capacity and plasticity in the common big-eared bat, *Micronycteris microtis* (Chiroptera: Phyllostomidae). PLoS One 6:e28584.
Santana S.E., Grosse I.R., Dumont E.R.. 2012. Dietary hardness, loading behavior, and the evolution of skull form in bats. Evolution 66:2587–2598.
Schöniger M., Von Haeseler A. 1994. A stochastic model for the evolution of autocorrelated DNA sequences. Mol. Phylogenet. Evol. 3:240–247.
Simmons M.P., Freudenstein J.V. 2003. The effects of increasing genetic distance on alignment of, and tree construction from, rDNA internal transcribed spacer sequences. Mol. Phylogenet. Evol. 26: 444–451.
Simmons N.B. 1996. A new species of *Micronycteris* (Chiroptera: Phyllostomidae) from northeastern Brazil, with comments on phylogenetic relationships. Am. Mus. Novit. 3158:1–35.
Simmons N.B. 1998. A reappraisal of interfamilial relationships of bats. In: Kunz T.H., Racey P.A., editors. Bats: phylogeny, morphology, echolocation and conservation. Washington (DC): Smithsonian Institution Press. p. 3–26.
Simmons N.B. 2005. Order Chiroptera. In: Wilson D.E., Reeder D.M., editors. Mammal species of the World: a taxonomic and geographic reference. Baltimore: Johns Hopkins University Press. p. 313–529.
Skelly D.A., Merrihew G.E., Riffle M., Connelly C.F., Kerr E.O., Johansson M., Jaschob D., Graczyk B., Shulman N.J., Wakefield J., Cooper S.J., Fields S., Noble W.S., Muller E.G.D., Davis T.N., Dunham M.J., MacCoss M.J., Akey J.M. 2013. Integrative phenomics reveals insight into the structure of phenotypic diversity in budding yeast. Genome Res. 23:1496–1504.
Smith S., Beaulieu J., Donoghue M. 2009. Mega-phylogeny approach for comparative biology: an alternative to supertree and supermatrix approaches. BMC Evol. Biol. 9:37.
Springer M.S., Burk-Herrick A., Meredith R., Eizirik E., Teeling E., O'Brien S.J., Murphy W.J. 2007. The adequacy of morphology for reconstructing the early history of placental mammals. Syst. Biol. 56:673–684.
Springer M.S., Meredith R.W., Eizirik E., Teeling E., Murphy W.J. 2008. Morphology and placental mammal phylogeny. Syst. Biol. 57: 499–503.
Springer M.S., Teeling E.C., Madsen O., Stanhope M.J., de Jong W.W. 2001. Integrated fossil and molecular data reconstruct bat echolocation. Proc. Natl Acad. Sci. USA 98:6241–6246.
Stamatakis A. 2006. RAxML-VI-HPC: maximum likelihood-based phylogenetic analyses with thousands of taxa and mixed models. Bioinformatics 22:2688–2690.
Stamatakis A., Hoover P., Rougemont J. 2008. A rapid bootstrap algorithm for the RAxML Web servers. Syst. Biol. 57:758–771.

Downloaded from https://academic.oup.com/sysbio/article/63/4/582/1623176 by guest on 20 August 2022

Swofford D.L. 2002. PAUP*. Phylogenetic analysis using parsimony (*and other methods). Sunderland (MA): Sinauer Associates.
Tavaré S. 1986. Some probabilistic and statistical problems on the analysis of DNA sequences. Lect. Math. Life Sci. 17:57–86.
Teeling E.C., Springer M.S., Madsen O., Bates P., O'Brien S.J., Murphy W.J. 2005. A molecular phylogeny for bats illuminates biogeography and the fossil record. Science 307:580–584.
Wagner P.J. 2000. Exhaustion of morphologic character states among fossil taxa. Evolution 54:365–386.
Wake D.B. 1991. Homoplasy: the result of natural selection, or evidence of design limitations? Am. Nat. 138:543–567.
Wetterer A.L., Rockman M.V., Simmons N.B. 2000. Phylogeny of phyllostomid bats (Mammalia: Chiroptera): data from diverse morphological systems, sex chromosomes, and restriction sites. Bull. Am. Mus. Nat. Hist. 248:1–200.
Wiens J.J. 2004. The role of morphological data in phylogeny reconstruction. Syst. Biol. 53:653–661.
Wiens J.J. 2009. Paleontology, genomics, and combined-data phylogenetics: can molecular data improve phylogeny estimation for fossil taxa? Syst. Biol. 58:87–99.
Wiens J.J., Chippindale P.T., Hillis D.M. 2003. When are phylogenetic analyses misled by convergence? A case study in Texas cave salamanders. Syst. Biol. 52:501–514.
Wiens J.J., Kuczynski C.A., Townsend T., Reeder T.W., Mulcahy D.G., Sites J.W. 2010. Combining phylogenomics and fossils in higher-level squamate reptile phylogeny: molecular data change the placement of fossil taxa. Syst. Biol. 59:674–688.
Wiens J.J., Moen D.S. 2008. Missing data and the accuracy of Bayesian phylogenetics. J. Syst. Evol. 46:307–314.
Wiens J.J., Tiu J. 2012. Highly incomplete taxa can rescue phylogenetic analyses from the negative impacts of limited taxon sampling. PLoS One 7:e42925.
Wilcoxon F. 1945. Individual comparisons by ranking methods. Biometr. Bull. 1:80–83.
Wilkinson M. 1995. A comparison of two methods of character construction. Cladistics 11:297–308.
Yang Z. 1994. Maximum likelihood phylogenetic estimation from DNA sequences with variable rates over sites: approximate methods. J. Mol. Evol. 39:306–314.
Zharkikh A. 1994. Estimation of evolutionary distances between nucleotide sequences. J. Mol. Evol. 39:315–329.

Downloaded from https://academic.oup.com/sysbio/article/63/4/582/1623176 by guest on 20 August 2022